University of South Carolina
Scholar Commons

Theses and Dissertations

Summer 2019

Implementation of View Factor Model and Radiative Heat Transfer Model in MOOSE

Abdurrahman Ozturk

Follow this and additional works at: https://scholarcommons.sc.edu/etd

Part of the Nuclear Engineering Commons

Recommended Citation

Ozturk, A.(2019). *Implementation of View Factor Model and Radiative Heat Transfer Model in MOOSE.* (Master's thesis). Retrieved from https://scholarcommons.sc.edu/etd/5348

This Open Access Thesis is brought to you by Scholar Commons. It has been accepted for inclusion in Theses and Dissertations by an authorized administrator of Scholar Commons. For more information, please contact dillarda@mailbox.sc.edu.

IMPLEMENTATION OF VIEW FACTOR MODEL AND RADIATIVE HEAT TRANSFER MODEL IN MOOSE

by

Abdurrahman Ozturk

Bachelor of Science
Hacettepe University, 2012

Submitted in Partial Fulfillment of the Requirements

For the Degree of Master of Science in

Nuclear Engineering

College of Engineering and Computing

University of South Carolina

2019

Accepted by:

Travis W. Knight, Director of Thesis

Benjamin Spencer, Reader

Cheryl L. Addy, Vice Provost and Dean of the Graduate School

© Copyright by Abdurrahman Ozturk, 2019
All Rights Reserved.

DEDICATION

This work is dedicated to my family who has never given up supporting me. I also want to dedicate this work to any person who has contribution on me during my life.

ACKNOWLEDGEMENTS

This material is based upon work partially supported by the U.S. Department of Energy NEUP IRP program under award agency number DE-NE-0008531. I also would like to acknowledge Dr. Travis W. Knight and Dr. Benjamin Spencer for his guidance and encouragement throughout the course of this research.

ABSTRACT

View factors are functions that represent the geometric relationship between surfaces. They are important parameters for radiative heat transfer calculations. View factor catalogues are available for simple geometries in the current literature. However, in the case of complicated geometry, analytical or numerical methods are needed to evaluate view factors. The Monte Carlo (MC) method is the most flexible one among numerical methods, which are used to calculate view factors, since it can be applied to any geometry.

When experimental studies are not affordable to conduct, modeling of engineering problems gains more importance. Idaho National Laboratory (INL)'s finite element framework Multiphysics Object Oriented Simulation Environment (MOOSE) is a robust engineering tool to model physical problems including heat transfer. However, MOOSE doesn't have a method to calculate view factors. Hence, a method is needed to calculate radiative heat transfer using view factors. Implementing a new model in MOOSE and using it in heat transfer calculations for an arbitrary geometry will enable the detailed evaluation of radiative heat transfer in complex geometries.

In this study, a nuclear fuel pellet heating and cracking experimental case is modeled as a sample case by using the new MOOSE methods that are implemented in this study. The effect of radiative heat transfer on radial and axial temperature profile is evaluated.

TABLE OF CONTENTS

DEDICATION iii

ACKNOWLEDGEMENTS iv

ABSTRACT v

LIST OF TABLES viii

LIST OF FIGURES ix

LIST OF SYMBOLS xii

LIST OF ABBREVIATIONS xiii

CHAPTER 1: INTRODUCTION AND MOTIVATION 1

CHAPTER 2: LITERATURE REVIEW 3

2.1. THEORY 3

2.2. LITERATURE REVIEWS 10

2.3. FINITE ELEMENT MODELING (MOOSE) 11

CHAPTER 3: METHODOLOGY 14

3.1. MONTE CARLO METHOD 14

3.2. MOOSE MESH STRUCTURE 14

3.3. MOOSE USER OBJECTS 16

3.4. VIEW FACTOR MODEL 17

3.5. RADIATIVE HEAT TRANSFER MODEL 48

CHAPTER 4: RESULTS AND DISCUSSION 50
4.1. PARALLEL RECTANGLES 51
4.2. PERPENDICULAR RECTRANGLES 55
4.3. COAXIAL DISKS 59
4.4. COAXIAL CYLINDERS 61
4.5. CONCENTRIC SPHERES 62
4.6. CASE STUDY: MODELING OF PELLET HEATING EXPERIMENT 63
CHAPTER 5: CONCLUSION 69
BIBLIOGRAPHY 70

LIST OF TABLES

Table 4.1 View Factors for h=2, w=2, d=2 51

Table 4.2 View Factors for different plate dimensions 54

Table 4.3 View Factors for h=3, w=3, d=4 56

Table 4.4 View Factors for different rectangle dimensions 58

Table 4.5 View factors for r_1=2, r_2=2, d=2 59

Table 4.6 View factors for different distance to radius ratio 59

Table 4.7 View factors for different disk dimensions 60

Table 4.8 View factors for r_1=1, r_2=2.5, h=6 61

Table 4.9 View factors for r_1=1, r_2=3 62

Table 4.10 Geometrical parameters for experimental setup 63

Table 4.11 Temperature Dependent UO_2 Thermal properties 64

Table 4.12 Thermal properties of materials 64

LIST OF FIGURES

Figure 2.1 An arbitrary black enclosure 4

Figure 2.2 Radiative exchange between two infinitesimal surface elements 6

Figure 2.3 Radiative exchange between two finite surfaces...7

Figure 3.1 Monte Carlo rays emitted from a source point..14

Figure 3.2 Fundamental parts of a finite element mesh..15

Figure 3.3 Side and node orientation for a hexahedron finite element.............................16

Figure 3.4 Length of a vector...18

Figure 3.5 Angle between vectors 19

Figure 3.6 Distance between points...20

Figure 3.7 Side map representation 21

Figure 3.8 Surface normal..22

Figure 3.9 Center point of element side...24

Figure 3.10 Area of a triangle..25

Figure 3.11 Area of element side by using triangles 26

Figure 3.12 Direction vector...27

Figure 3.13 Solid angle representation on spherical coordinates 28

Figure 3.14 Polar and Azimuthal Angle Distributions 29

Figure 3.15 Surface normal orientation 30

Figure 3.16 Unit normal vector in spherical coordinates...30

Figure 3.17 An arbitrary point on element side...34

Figure 3.18 An arbitrary point out of element side..34

Figure 3.19 Uniform distribution on a circle surrounding the element side......................35

Figure 3.20 Surface orientation...37

Figure 3.21 An arbitrary plane...39

Figure 3.22 Intersection point in spherical coordinates..40

Figure 3.23 Representation of source and intersection point..40

Figure 3.24 Testing intersection point on target surface...41

Figure 3.25 Testing visibility of target surface..43

Figure 3.26 Flow chart for Monte Carlo calculations..46

Figure 3.27 Flow chart for ViewFactor model 47

Figure 3.28 Radiative heat exchange between elements 48

Figure 3.29 Flow chart for RadiativeHeatFluxBC model..49

Figure 4.1 Geometry of parallel rectangles..51

Figure 4.2 View factor for parallel plates for different sampling number..........................52

Figure 4.3 Change of average view factor with sampling number.....................................52

Figure 4.4 Change in percentage error with sampling number...53

Figure 4.5 Change of average view factor with rectangle dimensions...............................54

Figure 4.6 Change of percentage error with rectangle dimensions 55

Figure 4.7 Geometry of perpendicular rectangles...55

Figure 4.8 Change of average view factor with sampling number.....................................56

Figure 4.9 Change of percentage error with sampling number 57

Figure 4.10 Change of average view factor with different rectangle dimensions 58

Figure 4.11 Geometry of coaxial disks 59

Figure 4.12 Change of average view factor with distance to radius ratio..........................60

Figure 4.13 Change of average view factor with disk radius 60

Figure 4.14 Geometry of coaxial cylinders..61

Figure 4.15 Geometry of concentric spheres 62

Figure 4.16 Geometry representation of experimental setup..63

Figure 4.17 Computation model of experimental setup...64

Figure 4.18 Pellet centerline temperature for only concentric cylinders 66

Figure 4.19 Pellet centerline temperature for computational geometry 67

Figure 4.20 Axial temperature profile in pellet 67

Figure 4.21 Radial temperature profile in pellet..68

LIST OF SYMBOLS

F	View factor
F_{ij}	View factor between surfaces i and j
q	Heat flux
Ω	Unit direction vector
n	Surface normal
N	Total number of sampled rays
m	Number of rays hitting target surface
E	Emissive Power

LIST OF ABBREVIATIONS

CDF.. Cumulative Distribution Function

FEM .... Finite Element Method

INL..Idaho National Laboratory

JFNK..Jacobian-free Newton Krylov

LWR...Light Water Reactor

MBM...MOOSE-BISON-MARMOT

MC .... Monte Carlo

MOOSE...Multiphysics Object Oriented Simulation Environment

PDF .... Probability Distribution Function

RIA..Reactivity Initiated Accident

TREAT..Transient Reactor Test Facility

USC...University of South Carolina

CHAPTER 1

INTRODUCTION AND MOTIVATION

Heat or energy is one of the main driving forces for transition from non-equilibrium state to steady state for a system. The system might be as complicated as a nuclear power plant or as simple as an ice cream. In almost all areas of science, it is essential to account for heat transfer to analyze the system correctly.

Heat is transferred by three mechanisms which are conduction in solids, convection of fluids and radiation between surfaces that are at high enough temperatures. In processes which require high temperatures such as power generation, combustion applications, heat treatment experiments and solar energy applications radiative heat transfer becomes significant and should be taken into consideration besides conduction and convection.[1]

In nuclear science, modeling is important because of the difficulty and safety concerns in experimental studies. Heat transfer, neutron transport, thermal hydraulic, fluid dynamics, material science are popular topics that researchers are developing computer codes to analyze systems. The finite element framework Multiphysics-Object-Oriented-Simulation-Environment (MOOSE), which is developed by Idaho National Laboratory (INL), is a powerful tool to model variety of engineering problems including nuclear science related problems such as fuel behavior under operating conditions. Since the temperature levels are very high for a nuclear reactor, the radiative heat transfer becomes dominant and should be modeled. Physically, radiative heat transfer occurs

between surfaces, so the geometric relationship between surfaces affects the heat exchange. However, the current radiative heat transfer model in MOOSE calculates heat transfer by assuming surfaces are infinitely parallel to each other and doesn't consider view factors in calculations.

In this research, it is aimed to implement new MOOSE models which are able to calculate the view factors and radiative heat transfer between surfaces. After literature review and doing some research to guide in choosing the right method, because of its applicability and feasibility for complex geometries, being one of the most efficient and commonly used numerical solution technique, Monte Carlo (MC) method is chosen in order to use in view factor calculations.

CHAPTER 2

LITERATURE REVIEW

2.1 THEORY

2.1.1 RADIATIVE HEAT TRANSFER

The radiative heat transfer is energy exchange between surfaces via electromagnetic waves. The heat coming from sun, feeling hot around camp fire can be given as everyday examples. All materials continuously emit and absorb electromagnetic waves or photons depending on surface temperature. The radiative heat transfer rates are generally proportional to differences in temperature of radiating materials to the fourth power. [1]

$$q \propto T^4 - T_\infty^4 \quad (1)$$

As it can be inferred from equation (1), the radiative heat transfer becomes dominant at high temperatures. Analyzing radiative heat transfer is more difficult compared to conduction and convection because of higher order temperature relation.

Electromagnetic waves striking a surface may be reflected, absorbed or transmitted. If the wave is attenuated in medium, then medium is called as opaque. If it passes through medium without attenuation, the medium is called as transparent. There is an important definition used in radiative heat transfer calculations: *black surface* or *black body*, which is an opaque surface does not reflect any radiation.

Another important term, *emissive power, (E),* is defined as the radiative heat flux emitted from a surface in all directions and calculated as,

$$E(T) = \int_0^\infty E_v(T,v)dv \tag{2}$$

and blackbody emissive power is calculated by Stefan-Boltzman Law,

$$E_b(T) = \int_0^\infty E_{bv}(T,v)dv = n^2\sigma T^4 \tag{3}$$

where $\sigma = 5.67e-8\frac{W}{m^2K^4}$ is known as Stefan-Boltzmann constant

n is refractive index ($n \cong 1$ for vacuum and gases)

To describe radiative heat flux leaving a surface, it is inadequate to use only emissive power. The direction dependent quantity, *radiative intensity, (I),* can be used instead.

$$I(r,\hat{s}) = \int_0^\infty I_\lambda(r,\hat{s},\lambda)d\lambda \tag{4}$$

Integrating radiative intensity over all possible directions will give total energy emission from surface,

$$E(r) = \int_{2\pi} I(r,\hat{s})\,\hat{n}\cdot\hat{s}\,d\Omega \tag{5}$$

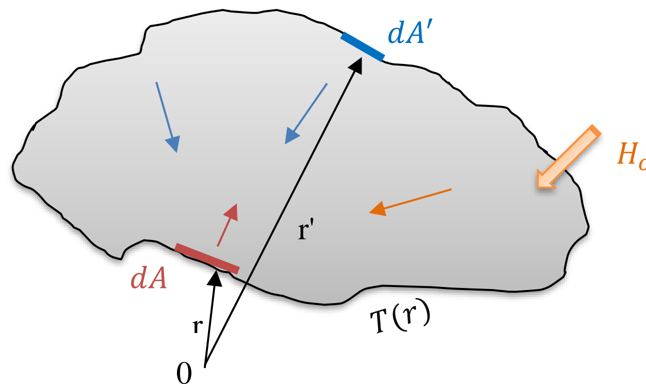

Figure 2.1 An arbitrary black enclosure

Figure 2.1 shows a black-walled enclosure of arbitrary geometry. The temperature distribution is indicated by $T(r)$. Energy balance for a small area of dA gives,

$$q(r) = E_b(r) - H(r) \tag{6}$$

$H(r)$ is the irradiation onto dA including both from entire enclosure and from outside.

$$H(r) = \int_A E_b(r')dF_{dA-dA'} + H_o(r) \tag{7}$$

$$q(r) = E_b(r) - \int_A E_b(r')dF_{dA-dA'} - H_o(r) \tag{8}$$

where $dF_{dA-dA'}$ is the view factor between surface dA and dA'.

If the enclosure is divided into N isothermal sub-surfaces, the average heat flux becomes

$$q_i = E_{bi} - \sum_{j=1}^{N} E_{bj}F_{i-j} - H_o(r) \tag{9}$$

where F_{i-j} is the view factor between surface A_i and A_j.

2.1.2 VIEW FACTORS

The radiative energy transfer between surfaces is nearly not affected by the medium that separates them. The participating media could be vacuum, monoatomic or diatomic gases at low temperatures. Such examples include solar collectors, radiative space heaters, illumination problems etc. Radiative heat exchange between surfaces can be analyzed by making assumptions of an idealized enclosure and surface properties. [1]

The most useful one is assuming that all surfaces are black, which means that there is no radiation reflection on surfaces and no direction dependency for radiation emission from surface. Reflection, absorption and transmission can be account for more realistic radiative heat transfer analyzes.

There is no range limit for thermal radiation, and if there is no participating media, photon will travel unimpeded from one surface to another. Therefore, no matter how far it is, surfaces can exchange radiative energy with one another. How much energy would be exchanged depends on surface areas, the distance separates them and their orientation. All these are represented by a geometric function called *view factor*. It is sometimes called as configuration factor, angle factor and shape factor. [1]

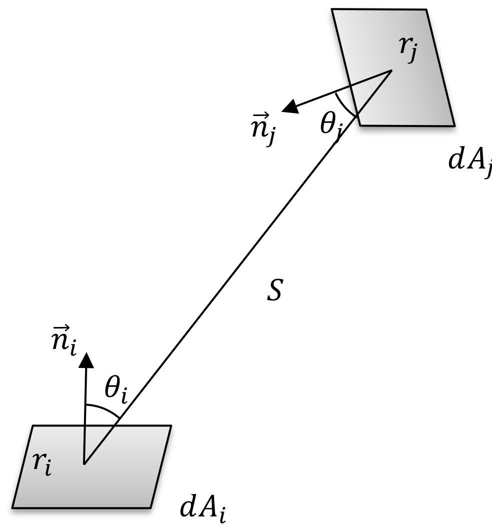

Figure 2.2 Radiative exchange between two infinitesimal surface elements

Figure 2.2 illustrates the radiative exchange between two infinitesimal surface elements dA_i and dA_j. The view factor for these surfaces determines how much energy leaves an arbitrary surface element toward the other one. For surface dA_i and dA_j in figure, view factor is defined as,

$$dF_{dA_i-dA_j} = \frac{diffuse\ energy\ leaving\ dA_i\ directly\ toward\ and\ intercepted\ dA_j}{total\ diffuse\ energy\ leaving\ dA_i} \quad (10)$$

the heat transfer rate from dA_i to dA_j is determined by the radiative intensity as,

$$I(r_i)(dA_i \cos\theta_i)d\Omega_j = \frac{I(r_i)\cos\theta_i \cos\theta_j \, dA_i dA_j}{S^2} \tag{11}$$

total radiative energy leaving dA_i is called as *radiosity* and related to intensity as

$$J(r_i)dA_i = [E(r_i) + \rho(r_i)H(r_i)]dA_i = \pi I(r_i)dA_i \tag{12}$$

Then view factor between two infinitesimal diffuse surfaces is

$$dF_{dA_i-dA_j} = \frac{\cos\theta_i \cos\theta_j}{\pi S^2} dA_j \tag{13}$$

The view factors have an important rule called law of reciprocity which is derived from the equation (13), and it says

$$dA_i dF_{dA_i-dA_j} = dA_j dF_{dA_i-dA_j} \tag{14}$$

The definition of view factor can be expanded to include radiative change between two finite surfaces shown in Figure 2.3.

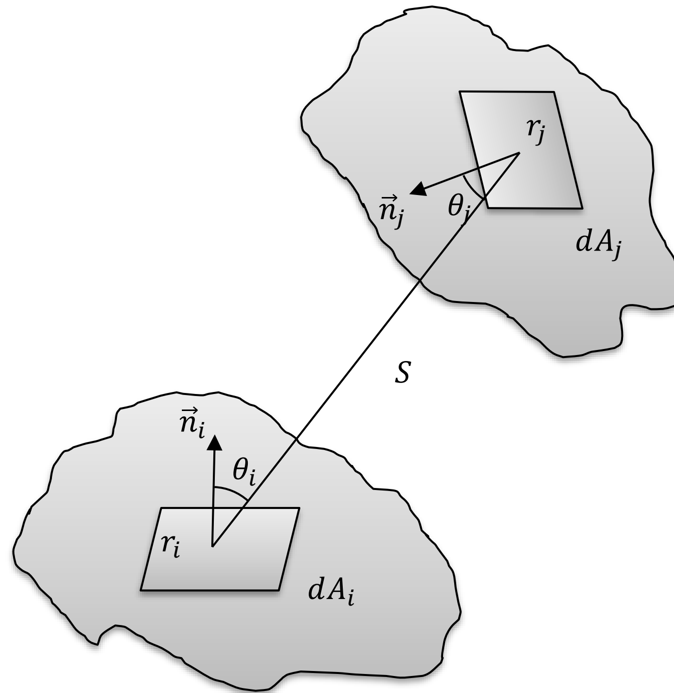

Figure 2.3 Radiative exchange between two finite surfaces

Similarly, the total energy leaving A_i toward A_j is,

$$\int_{A_i} \int_{A_j} I(r_i) \frac{\cos\theta_i \cos\theta_j}{S^2} dA_j dA_i \tag{15}$$

and view factor is defined as

$$F_{A_i - A_j} = \frac{\int_{A_i} \int_{A_j} I(r_i) \frac{\cos\theta_i \cos\theta_j}{S^2} dA_j dA_i}{\pi \int_{A_j} I(r_i) dA_i} \tag{16}$$

If it is assumed that the intensity leaving A_i does not vary across the surface, the view factor reduces to,

$$F_{A_i - A_j} = \frac{1}{A_i} \int_{A_i} \int_{A_j} \frac{\cos\theta_i \cos\theta_j}{\pi S^2} dA_j dA_i \tag{17}$$

Then another version of the law of reciprocity is found,

$$A_i F_{A_i - A_j} = A_j F_{A_j - A_i} \tag{18}$$

If the surface is a part of enclosure geometry, there is also a summation relationship for view factors,

$$\sum_{j=1}^{N} F_{di-j} = \sum_{j=1}^{N} F_{i-j} = 1 \tag{19}$$

2.1.3 METHODS FOR VIEW FACTOR CALCULATIONS

The calculation of view factor between two specified surfaces requires to solve the double area integral given in equation (17). Analytical solution of such kind of integrals is not easy to evaluate for complex geometries. Therefore, analytical approaches or numerical methods are used to handle view factor calculations.

Evaluation methods for view factors can be categorized into three groups,

1- Direct integration

2- Special methods

3- Statistical determination

The view factor formula (Eq. (17)) can be solved directly by numerical or analytical integration methods if the geometry is not too complicated. Area integration and contour integration are known methods for direct integration. Furthermore, there are special methods using view factor algebra, including reciprocity and summation rules, instead of calculating integration.

Experimental methods can also be used to calculate view factors. Unit sphere method introduced as the first experimental method by Nusselt in 1928. It is a powerful method to calculate view factors between one infinitesimal and one finite area. Later on, ray casting method was developed based on unit sphere method, which is using computer graphics technique to construct the projected area. [1]

Another way to calculate view factors is statistical sampling with Monte Carlo (MC) method. MC method is a class of numerical techniques based on the statistical characteristics of physical models. The method was developed by early workers trying to analyze the potential behavior of nuclear weapons. Experiments were difficult and analysis methods were not able to provide accurate prediction. Thus, simulating neutrons and tracking their behavior was the solution to understand average weapon behavior. An early description of the philosophy behind the MC approach was given by Metropolis and Ulam (1949) [2].

In view factor calculations, a total number of rays (N) are emitted from a surface with identical properties but random directions. Some of the rays will hit target surface while others will not. If the number of rays hit is m, then view factor is calculated as,

$$F_{ij} = \frac{m}{N} \tag{20}$$

2.2 LITERATURE REVIEWS

In literature there are many works done by researchers for view factor calculations. Different methods were tested for complex geometries for which theoretical formulas cannot be used.

Bopche and Sridharan (2009) presented an application of contour integral technique to calculation of diffuse view factors for elements of nuclear fuel bundle. They derived analytical expressions for different cases including two identical cylindrical rods, two cylindrical rods with interference by another rod, and between one cylindrical rod and a non-concentric cylindrical enclosure. They compared results obtain from their expressions with literature and concluded that using infinite length approximations in finite length calculations can cause high computational errors. [7]

Narayanaswamy (2015) has used Nusselt’s unit sphere method to calculate view factor between two arbitrarily oriented planar triangles and planar polygons. The main reason of focusing only these two arbitrary shapes was that most mesh generation software for finite element analysis and computer graphics discretize geometry into them. He ended up with deriving an expression for view factor between two arbitrarily oriented planar polygons, which obeying reciprocity rule of view factors. Another conclusion of this study was that the numerical quadrature is not

needed for evaluation of the special function in the analytical view factor expression.[8]

Lei Yang and Wenzhen Chen (2014) thought that existing theoretical formulas for view factor between nuclear fuel bundles are not suitable for non-standard assembly geometries such as hexagonal or circular. For view factor calculations, they used discrete transfer model (DTRM) and discrete ordinates model (DO), which both are proposed on CFD method. They concluded that DTRM method can be used to calculate view factors accurately. [9].

Barry and Ying (2016) calculated numerically view factors between hot and cold side ceramic plates within a thermoelectric device with ray tracing method by utilizing hybrid CPU-GPU high performance computing. They tried different set of dimensions for plates and obtain very accurate results. [10]

Mirhosseini and Saboonchi (2011) applied the MC method to calculate view factors for a plate including strip elements to circular. They investigated the performance of MC technique by changing number of strip elements and number of rays. They observed that the error decreased as the number of rays increased, which was expected for a statistical method.[11]

2.3 FINITE ELEMENT MODELING (MOOSE)

Modeling physical problems is a powerful way for engineers and scientists to understand the nature of the problem. Computational models can bring light for special cases that are difficult measure experimentally. Especially in nuclear industry, because of safety and cost related concerns, computational studies take an important place.

Every phenomenon in nature can be described by the laws of physics with terms of algebraic, differential, and/or integral equations, which is called analytical description of physical phenomenon or mathematical models. The solution of mathematical models is sometimes not easy to solve and requires making reasonable assumptions or using numerical methods. Rapid development in computer science makes it possible to solve many engineering problems numerically. [4]

The finite element method and its generalizations are the most powerful computer-oriented methods ever devised to analyze practical engineering problems. Today, finite element analysis has a significant place in many fields of engineering design and manufacturing. [4]

In finite element, first, the geometry of problem is divided into subdomains or finite elements. Then, for each element, governing equations that represent the physics of the problem are approximated by polynomials. Finally, the equations are solved, and an approximate solution is found on finite elements.

Multiphysics Object Oriented Simulation Environment (MOOSE) is a parallel computational framework has been under development since 2008 to provide solutions to systems of coupled, nonlinear partial differential equations (PDEs) which are important for nuclear processes. Differ from traditional data-flow oriented computational frameworks, MOOSE uses Jacobian-free Newton-Krylov (JFNK) scheme in order to reduce memory and time consumption. This scheme employs Krylov method for solving the linear system that result from the application of Newton’s method. Since the Krylov iterative methods require only matrix-vector product rather than full matrix product, the full Jacobian matrix is not needed. [5]

Starting with a discrete problem of length N,

$$F(x) = 0 \tag{21}$$

the Jacobian of the system is defined by the $N\ x\ N$ matrix

$$\mathcal{J}(x) = \frac{\partial F(x)}{\partial x} \tag{22}$$

The Newton iteration can be expressed as

$$\mathcal{J}(x^k)\delta x^k = -F(x^k) \tag{23}$$

which leads to

$$x^{k+1} = x^k + \partial x^k \tag{24}$$

By using Krylov solvers, the Jacobian matrix is reduced to a matrix-vector

$$\mathcal{J}(x^k)\delta x^k \approx \frac{F(x^k + \epsilon\delta x^k) - F(x^k)}{\epsilon} \tag{25}$$

CHAPTER 3

METHODOLOGY

3.1 MONTE CARLO METHOD

Like other MC applications, rays used in view factor calculations are sampled from an origin, and their behavior is tracked till they are disappeared. Rays are considered as having identical properties except direction. In this work, rays are considered as absorbed in the first surface they intersect. Figure 3.1 illustrates MC rays used to calculate view factor between parallel plates.

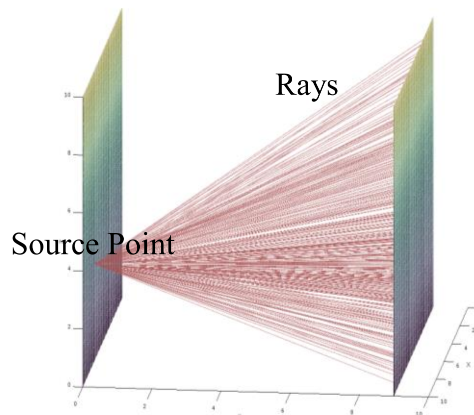

Figure 3.1 Monte Carlo rays emitted from a source point

3.2 MOOSE MESH STRUCTURE

MOOSE has a built-in mesh generator for simple meshes such as lines, rectangles, and rectangular prisms(boxes). For complex geometries, it is suggested to use external mesh generation software and convert it to a format that MOOSE can read.

Finite element mesh is formed by four main parts: blocks, elements, sides and nodes. In Figure 3.2, these fundamental parts are illustrated to make them easy to understand. The 3D cubic mesh in figure was generated by using Trelis.

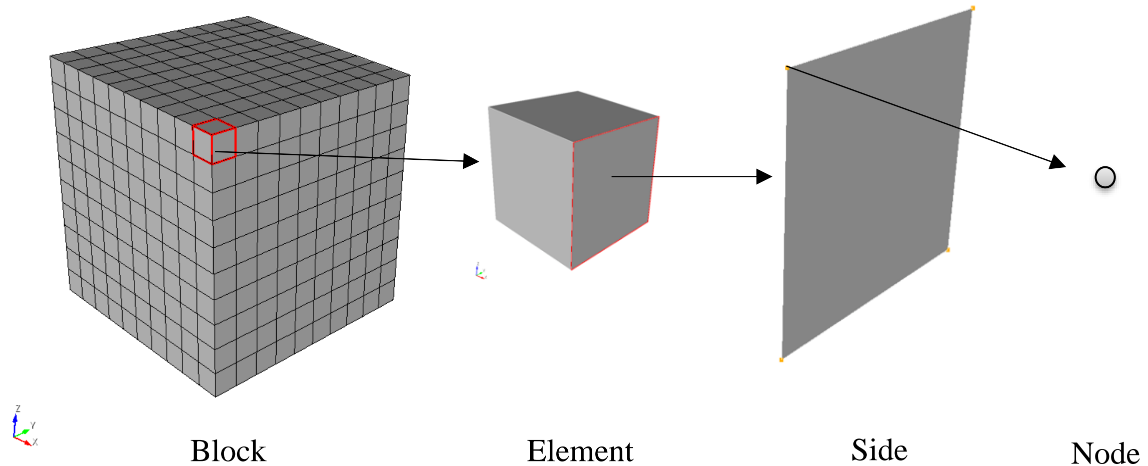

Figure 3.2 Fundamental parts of a finite element mesh.

For this mesh, there is only one mesh block, and 8-noded hexahedron (HEX8) is chosen as element type. The block has 1000 finite elements (10x10x10), each finite element has 6 sides, and each side has 4 nodes. Number of sides and nodes might change according to element type such tetrahedron, pentahedron.

In MOOSE mesh structure, blocks, block sides(boundaries) and elements have unique identification (ID) numbers. On the other hand, elements' sides and nodes do not have any unique IDs because they vary on the element type. Instead, they are identified in counter-clockwise order, as described in Figure 3.3.

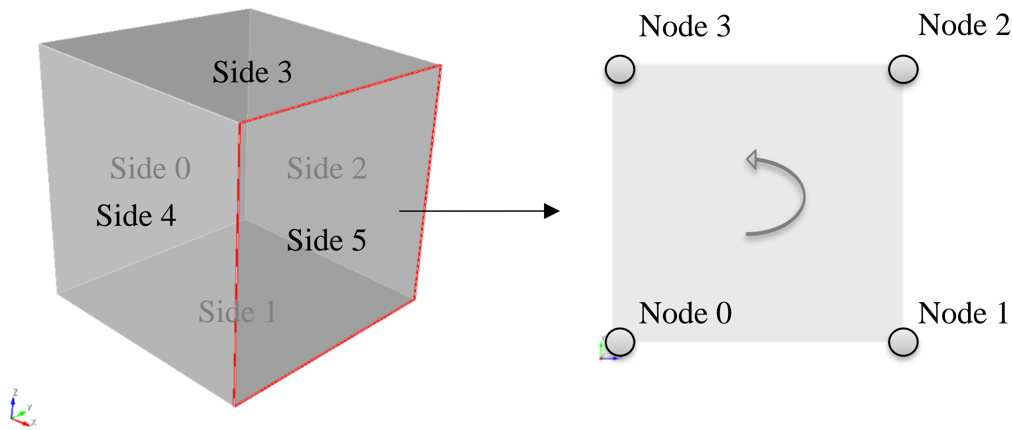

Figure 3.3 Side and node orientation for a hexahedron finite element.

3.3 MOOSE USEROBJECT

UserObject is a system in MOOSE framework that defines its own interface, which other MOOSE objects can call to retrieve data. It can provide results as scalar or vector value to other MOOSE objects. Users can easily add their own user objects to perform any kind of calculation. There are four types of UserObjects:

- ElementUserObject: performs evaluations on each element;
- NodalUserObject: performs evaluations on each node;
- SideUserObject: performs evaluations on each side; and
- GeneralUserObject: is a generic object that can do any calculation while providing a common interface for use by other MOOSE objects.

UserObjects have a specific anatomy and must override following functions,

- virtual void initialize(): it is called just ones before starting calculations. This is useful for resetting data structures and initializing one-time variables such as pseudo-random number seed.

- virtual void execute(): it is called once on each geometric object(element,node or side) or just one time per calculation for a GeneralUserObject. All calculations are done inside this function.
- virtual void threadJoin(const UserObject &y): it is used during threaded execution to join together calculations generated on different threads. the “y” needs to be casted to a constant reference of type of UserObject itself, then the data from “y” needs to be extracted and added to the data in current(this) object.
- virtual void finalize(): it is the very last function called after all calculations have been completed. The user must take all of the calculations performed in execute() and do some last operation to get final values.
- In addition to these functions, to provide data or result to other MOOSE objects, an accessor function is defined, allowing for other MOOSE object can call this function and get the result of the calculations done by user object. The accessor function can be named as getValue(), averageValue(), etc…

3.4 VIEW FACTOR MODEL

Since it is extremely powerful and flexible, user object system is chosen to calculate view factors. The implemented user object model is named as “ViewFactor”. It is a derived class inheriting from a base class “ViewFactorBase”, which keeps all user defined variables and user defined functions. All geometrical calculations, linear algebra operations and MC sampling are done via user defined functions. It is safer and easier to understand the code when functions are used instead of writing the whole code in just one

complex script. All user defined functions used in this work, and the physics behind them are explained in details in this section.

ViewFactorBase class contains the following functions,

- getSideMap(elemPTR,sideID)
- getNormal(sideMap)
- getCenterPoint(sideMap)
- getArea(point, sideMap)
- getRandomDirection(normal, dimension)
- isOnSurface(point, sideMap)
- getRandomPoint(sideMap)
- isIntersected(point, direction, sideMap)
- isSidetoSide(sideMap, sideMap)
- isVisible(sideMap, sideMap)
- doMonteCarlo(sideMap, sideMap, sourceNumber, samplingNumber)

3.4.1 VECTOR LENGTH

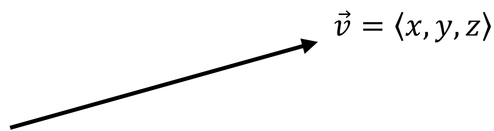

Figure 3.4 Length of a vector

Vector is an object that has a magnitude and direction in space, having valuable information for geometrical calculations. The magnitude (length) of a vector $\vec{v} = \langle x, y, z \rangle$ shown in Figure 3.4, $\|\vec{v}\|$, can be calculated by following formula.

$$\|\vec{v}\| = \sqrt{x^2 + y^2 + z^2} \tag{26}$$

The function norm() in Point class is using this equation to calculate vector magnitude.

```
const Point v;
Real vector_length = v.norm()
```

3.4.2 ANGLE BETWEEN VECTORS

The angle between two vectors can be calculated by using the cosine formula.

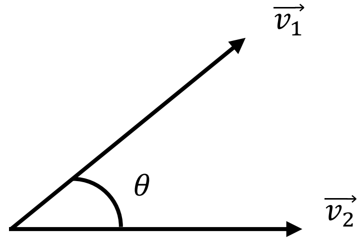

Figure 3.5 Angle between vectors

$$cos\theta = \frac{(\overrightarrow{v_1} \cdot \overrightarrow{v_2})}{\|\overrightarrow{v_1}\|\|\overrightarrow{v_2}\|} \tag{27}$$

where $\|\overrightarrow{v_1}\|$ and $\|\overrightarrow{v_2}\|$ are the lengths of vectors $\overrightarrow{v_1} = \langle x_1, y_1, z_1 \rangle$ and $\overrightarrow{v_2} = \langle x_2, y_2, z_2 \rangle$, respectively, and $(\overrightarrow{v_1} \cdot \overrightarrow{v_2})$ is the dot product of the $\overrightarrow{v_1}$ and $\overrightarrow{v_2}$ vectors, defined as:

$$(\overrightarrow{v_1} \cdot \overrightarrow{v_2}) = x_1x_2 + y_1y_2 + z_1z_2 \tag{28}$$

Afterwards, the angle between vectors $\overrightarrow{v_1}$ and $\overrightarrow{v_2}$ can be calculated by using arccosine:

$$\theta = \mathrm{acos}\left(\frac{(\overrightarrow{v_1} \cdot \overrightarrow{v_2})}{\|\overrightarrow{v_1}\|\|\overrightarrow{v_2}\|}\right) = acos\left(\frac{x_1x_2 + y_1y_2 + z_1z_2}{\sqrt{(x_1^2 + y_1^2 + z_1^2)(x_2^2 + y_2^2 + z_2^2)}}\right) \tag{29}$$

```
const Point v1;
const Point v2;
const Real theta = acos((v1*v2)/(v1.norm()*v2.norm()));
```

3.4.3 DISTANCE BETWEEN POINTS

The distance between two points in space is calculated by using following formula;

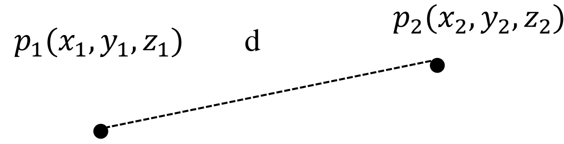

Figure 3.6 Distance between points

$$d = \sqrt{(x_2 - x_1)^2 + (y_2 - y_1)^2 + (z_2 - z_1)^2} \tag{30}$$

The distance between points is equal the magnitude of vector that is created by points.

```
const Point v1;
const Point v2;
const Real d = (v2-v1).norm();
```

3.4.4 ELEMENT SIDE MAP FOR NODAL COORDINATES

Map is one of the useful associative containers in C++ Standard Template Library (STL). It contains key/value pairs, where key serves as an index into the map, and the value serves as the associated data to be stored. The value can be any type in C++, so map of containers such as map of vectors or map of maps can be defined.

In this work, to store nodal coordinates of element sides, map of vectors, which is compatible with any kind of element type, is used, and termed as “side_map”. In almost all functions, side_map is used as function argument. The key of side_map is an integer and represents node ID in element side. The value of side_map is a vector and represents the Cartesian (x,y,z) coordinates of the associated node. The size of side_map is equal to

the number of nodes on element side. Figure 3.7 illustrates what side_map represents for an element side.

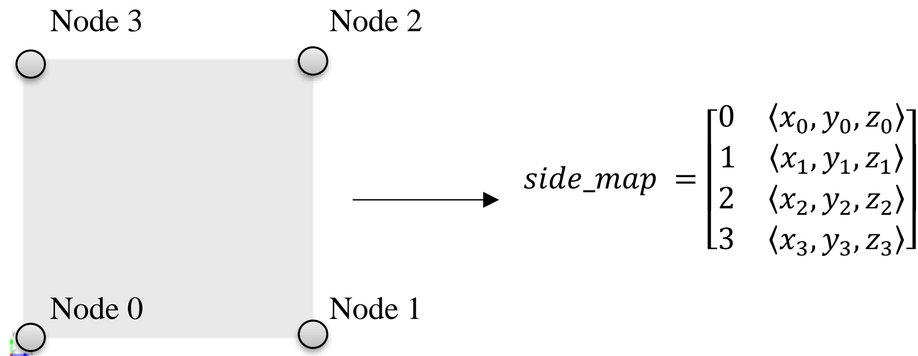

Figure 3.7 Side map representation

MOOSE is an object-oriented framework written in C++, giving the opportunity to create individual objects for each element, side and node. Using pointers is the best way to access these objects to reduce memory usage. View factor calculations are related to element sides, and thus, side pointers are needed to retrieve nodal coordinates from element surfaces. The UserObject model, ViewFactor, is inheriting from SideUserObject class, which automatically loops over all elements in a specified boundary. For each iteration of the loop, pointers are created to current element object.

Element object in MOOSE has a useful member function which creates a pointer to side of an element if associated side ID is passed to function as argument. Similarly, side object in MOOSE has a member function to create pointer to nodes of the side by passing node ID to function. Those node pointers can be used to access nodal coordinates. “side_map” is created by looping over nodes on a side and inserting their IDs and x,y,z coordinates to map container.

The function getSideMap(elemPTR,sideID) in ViewFactorBase class is using element pointer and side ID and creates side_map as explanied.

```
const std::map<unsigned int, std::vector<Point>>
ViewFactorBase::getSideMap(const Elem * elem,const unsigned int
side) const
{
  auto elem_side-elem->build_side_ptr(side);
  std::map<unsigned int, std::vector<Point>> side_map;
  unsigned int n_n = elem_side->n_nodes();
  for (unsigned int i = 0; i < n_n; i++)
  {
    const Node * node = elem_side->node_ptr(i);
    Point node_p((*node)(0), (*node)(1), (*node)(2));
    side_map[i].push_back(node_p);
  }
  return side_map;
}
```

3.4.5 ELEMENT SIDE NORMAL

Surface normal $\vec{n}$, plays an important role in view factor calculations; it is always orthogonal to a surface, and hence it is perpendicular to any point or vector lie on the surface. For finite element mesh, normal is prone to change according to element side. $\vec{n}$ can be found by cross product of any given two vectors, defined by three arbitrary points on the surface.

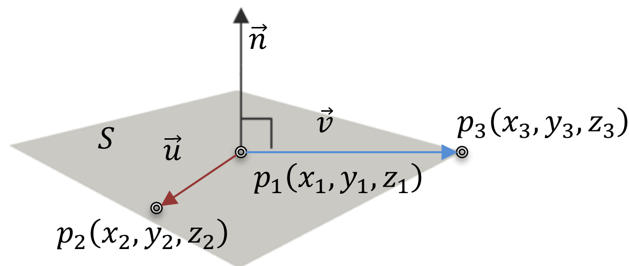

Figure 3.8 Surface normal

For instance, in Figure 3.8, p_1, p_2, p_3 are random points on surface S, vectors u and v are calculated by taking difference point coordinates.

$$\vec{u} = \langle u_x, u_y, u_z \rangle = \langle p3 - p1 \rangle = \langle (x_3 - x_1), (y_3 - y_1), (z_3 - z_1) \rangle$$

$$\vec{v} = \langle v_x, v_y, v_z \rangle = \langle p2 - p1 \rangle = \langle (x_2 - x_1), (y_2 - y_1), (z_2 - z_1) \rangle$$

Then surface normal is calculated as,

$$\vec{n} = \vec{u} \times \vec{v} = det \begin{vmatrix} i & j & k \\ u_x & u_y & u_z \\ v_x & v_y & v_z \end{vmatrix}$$

$$\vec{n} = \left(u_y v_z - u_z v_y\right)i - \left(u_x v_z - u_z v_x\right)j + \left(u_x v_y - u_y v_x\right)k \tag{31}$$

The function getNormal(sideMap) in ViewFactorBase class is calculating surface normal in this way. It takes side_map as function argument, and uses first three nodes as random points in an element surface, and uses them to calculate the surface normal. After normalization, it returns surface normal as unit vector.

```
const Point
ViewFactorBase::getNormal(std::map<unsigned int,
std::vector<Point>> map) const
{
  Point p1 = map[0][0];
  Point p2 = map[1][0];
  Point p3 = map[2][0];
  Point v12(p2-p1);
  Point v13(p3-p1);
  Point n(v12.cross(v13));
  n /= n.norm();
  return n;
}
```

3.4.6 CENTER POINT OF ELEMENT SIDE

The geometric center point or centroid of a surface is useful for calculating area and sampling a random point on a surface. Centroid can be calculated by finding arithmetic mean position of all points surrounding polygon.

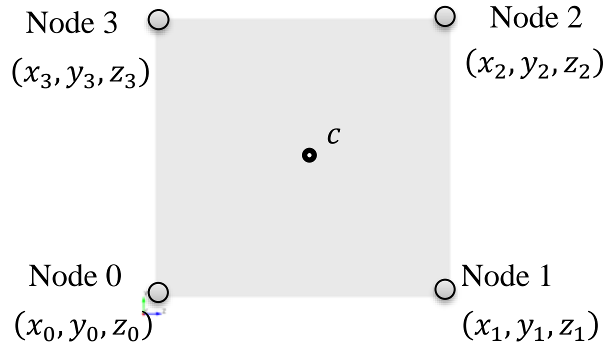

Figure 3.9 Center point of element side

For a 4 noded-element side in Figure 3.9, center point can be calculated as,

$$c = \left(\left(\frac{\sum_{i=0}^{n=3} x_i}{4} \right), \left(\frac{\sum_{i=0}^{n=3} y_i}{4} \right), \left(\frac{\sum_{i=0}^{n=3} z_i}{4} \right) \right) \tag{32}$$

The function getCenterPoint(sideMap) in ViewFactorBase class calculates the center point of element side when side_map is passed to function and returns as a vector.

```
const Point
ViewFactorBase::getCenterPoint(std::map<unsigned int,
std::vector<Point> > map) const
{
  unsigned int n=map.size();
  Point center(0,0,0);
  for (size_t i = 0; i < n; i++)
  {
    center += map[i][0];
  }
  center /= n;
  return center;
}
```

3.4.7 ELEMENT SIDE AREA CALCULATIONS

Surface area is another important parameter for view factor calculations. One of the simplest approaches to calculate the area of any polygon is dividing the polygon to triangles, afterwards calculating their areas and finally summing the areas of triangles. In

linear algebra, the area of a triangle can be calculated by finding half of the magnitude of the cross-product of two edges.

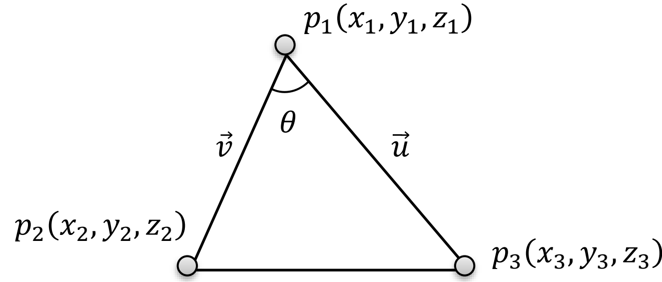

Figure 3.10 Area of a triangle

$$\vec{u} = \langle u_x, u_y, u_z \rangle = \langle p3 - p1 \rangle = \langle (x_3 - x_1), (y_3 - y_1), (z_3 - z_1) \rangle$$

$$\vec{v} = \langle v_x, v_y, v_z \rangle = \langle p2 - p1 \rangle = \langle (x_2 - x_1), (y_2 - y_1), (z_2 - z_1) \rangle$$

$$S = \frac{|\vec{u} \times \vec{v}|}{2} = \frac{|\vec{u}||\vec{v}|sin\theta}{2} \quad (33)$$

The vector lengths and the angle between vectors can be calculated by using functions getVectorLength() and getAngleBetweenVectors(), which are using equations (26) and (29).

The element side area can be calculated by dividing into triangles, following the previously discussed method. An arbitrary point is needed to create triangles by pairing it with nodes. The center point of an element side can be used to create triangles as shown in Figure 3.11. getCenterPoint() function will provide coordinates of center points when side_map is passed as an argument.

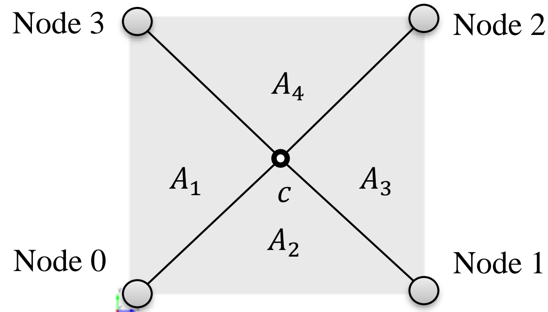

Figure 3.11 Area of element side by using triangles

The function getArea(point,sideMap) in ViewFactorBase class calculates total area of triangles created by a given point and side nodes. When the point and side_map is passed to function, it calculates and returns total area.

```
const Real
ViewFactorBase::getArea(const Point &p, std::map<unsigned int,
std::vector<Point>> map) const
{
  unsigned int n = map.size();
  Real area{0};
  for (size_t i = 0; i < n; i++)
  {
    const Point node1 = map[i][0];
    const Point node2 = map[(i+1)%n][0];
    const Point v1(node1-p);
    const Point v2(node2-p);
    const Real theta = acos((v1*v2)/(v1.norm()*v2.norm()));
    area += 0.5 * v1.norm() * v2.norm() * sin(theta);
  }
  return area;
}
```

3.4.8 SAMPLING RANDOM DIRECTION

Direction sampling is one of the most important part of view factor calculations in this work, in which a direction is sampled randomly in spherical coordinates system. In spherical coordinate system, a direction vector is defined by length, r, polar angle, θ, and

azimuthal angle, ϕ. The Figure 3.12 shows conversion of a unit direction vector from global spherical coordinate system to global cartesian coordinate system, Ω.

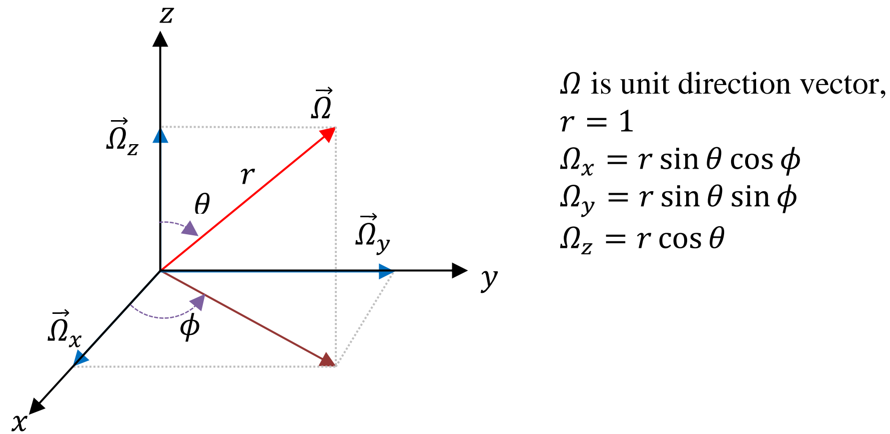

Figure 3.12 Direction vector

The polar angle changes from 0 to π, and the azimuthal angle from 0 to 2π. Direction vector can be found once the angles have been specified in these intervals. However, the angles should be selected carefully to obtain a uniform direction distribution at a given radial position. In spherical coordinate system vectors moves away from each other in radial direction. Because of this, random numbers cannot be used directly to sample angles in their ranges. Instead, probability distribution functions(PDF) needs to be defined correctly and then cumulative distribution functions(CDF) needs to be determined and used to sample angles uniformly.

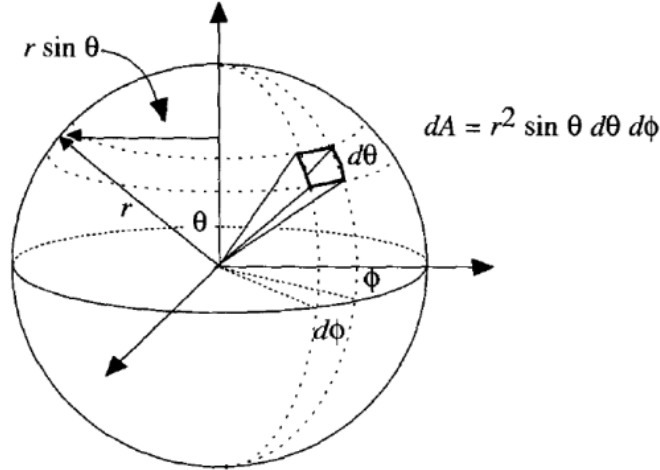

Figure 3.13 Solid angle representation on spherical coordinates

The Figure 3.13 shows a uniformly distributed points on a sphere surface. The basic idea to obtain a uniform distribution is to consider the points to be photons or particles that are emitted from an isotropic source. In that case, each element of a solid angle should receive the same contribution from source, so the ratio of the unit element area to sphere surface area, which is equal for each of photon(particle), relates to the PDF.

$$PDF(\theta,\phi)d\theta d\phi = \frac{dA}{A}$$

$$PDF(\theta,\phi)d\theta d\phi = \frac{r^2 \sin\theta \, d\theta d\phi}{4\pi r^2}$$

$$PDF(\theta)d\theta \, . \, PDF(\phi)d\phi = \frac{\sin\theta \, d\theta}{2}\frac{d\phi}{2\pi}$$

$$PDF(\theta)d\theta = \frac{\sin\theta \, d\theta}{2} \quad \rightarrow \quad \int_0^{\pi} PDF(\theta)d\theta = \int_0^{\pi} \frac{\sin\theta \, d\theta}{2} = 1 \qquad (34a)$$

$$PDF(\phi)d\phi = \frac{d\phi}{2\pi} \quad \rightarrow \quad \int_0^{\pi} PDF(\phi)d\phi = \int_0^{2\pi} \frac{d\phi}{2\pi} = 1 \qquad (34b)$$

$$CDF(\theta) = \int_0^\theta PDF(\theta)d\theta = \int_0^\theta \frac{\sin\theta\, d\theta}{2} = \frac{1-\cos\theta}{2} \tag{35a}$$

$$CDF(\phi) = \int_0^\phi PDF(\phi)d\phi = \int_0^\phi \frac{d\phi}{2\pi} = \frac{\phi}{2\pi} \tag{35b}$$

Cumulative distribution functions are uniformly distributed random numbers, and thus, the θ and ϕ distributions, shown in Figure 3. 14, now can be calculated indirectly by using random numbers.

$$\xi_1 = CDF(\theta) = \frac{1-\cos\theta}{2} \;\rightarrow\; \theta = \text{acos}(1-2\xi_1) \tag{36a}$$

$$\xi_2 = CDF(\phi) = \frac{\phi}{2\pi} \;\rightarrow\; \phi = 2\pi\xi_2 \tag{36b}$$

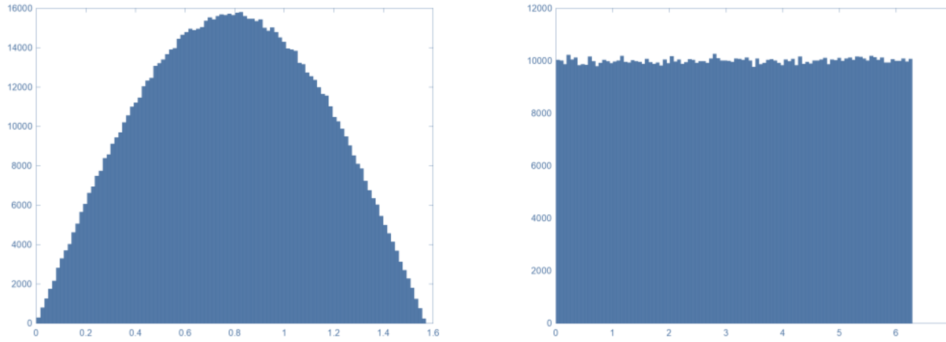

Figure 3.14 Polar Angle, θ and Azimuthal Angle, ϕ Distributions

These distribution functions ensure directions are uniformly distributed and can be used in view factor calculations. In addition to uniform direction distribution, the coordinate system is important for sampling as well. Finite element mesh has different sides and they are not necessarily aligned with the global coordinate system, shown in Figure 3.15 Instead, a local coordinate system can be used for direction sampling to make it compatible with any element side.

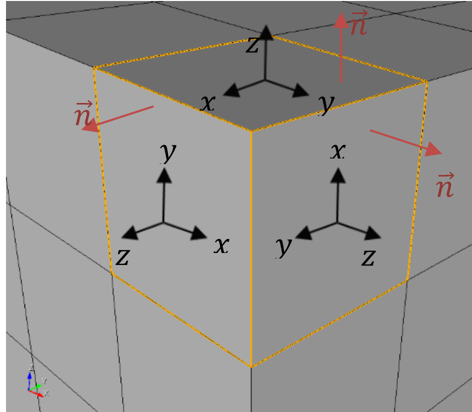

Figure 3.15 Surface normal orientation

Local coordinate system is basically created by rotating global coordinate system till z-axis is aligned with the surface normal vector. The rotation angles are recorded for later use in rotation matrix. Direction vector is sampled in global coordinate system as previously described, and then by applying rotation matrix, it is transformed to local coordinate system.

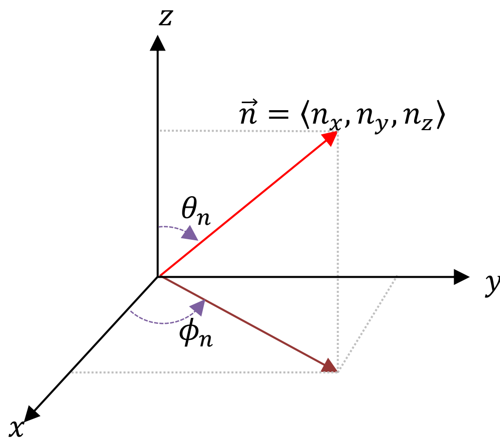

n is unit normal vector,

$$\theta_n = \operatorname{acos}(n_z)$$

$$\phi_n = \operatorname{acos}\left(\frac{n_x}{\sin\theta_n}\right) \qquad \text{for } (n_y > 0)$$

$$\phi_n = 2\pi - \operatorname{acos}\left(\frac{n_x}{\sin\theta_n}\right) \qquad \text{for } (n_y < 0)$$

Figure 3.16 Unit normal vector in spherical coordinates

Rotation matrix is generated by using negative angles of unit normal vector.

$$\theta_l = -\theta_n = -\mathrm{acos}(n_z)$$

$$\phi_l = -\phi_n = -\,\mathrm{acos}\left(\frac{n_x}{\sin\theta_n}\right)$$

$$R_z = \begin{bmatrix} \cos\phi_l & \sin\phi_l & 0 \\ -\sin\phi_l & \cos\phi_l & 0 \\ 0 & 0 & 1 \end{bmatrix} \quad , \quad R_y = \begin{bmatrix} \cos\theta_l & 0 & -\sin\theta_l \\ 0 & 1 & 0 \\ \sin\theta_l & 0 & \cos\theta_l \end{bmatrix}$$

$$R_{local} = R_z * R_y = \begin{bmatrix} \cos\theta_l\cos\phi_l & \sin\phi_l & -\cos\phi_l\sin\theta_l \\ -\cos\theta_l\sin\phi_l & \cos\phi_l & \sin\theta_l\cos\phi_l \\ \sin\theta_l & 0 & \cos\theta_l \end{bmatrix} \tag{37}$$

In the final step, the unit direction vector(Ω_g) is sampled in global coordinate system then transformed to local coordinate system (Ω_l) by multiplying it with the rotation matrix. If 2D direction is requested, polar angle(θ) is assumed as $\pi/2$, making it parallel to the surface normal vector.

$$\Omega_g = \begin{bmatrix} \Omega_x \\ \Omega_y \\ \Omega_z \end{bmatrix} = \begin{bmatrix} \sin\theta\cos\phi \\ \sin\theta\sin\phi \\ \cos\theta \end{bmatrix}$$

$$R_{local} = \begin{bmatrix} \cos\theta_l\cos\phi_l & \sin\phi_l & -\cos\phi_l\sin\theta_l \\ -\cos\theta_l\sin\phi_l & \cos\phi_l & \sin\theta_l\cos\phi_l \\ \sin\theta_l & 0 & \cos\theta_l \end{bmatrix}$$

$$\Omega_l = R_{local}\Omega_g = \begin{bmatrix} \cos\theta_l\cos\phi_l & \sin\phi_l & -\cos\phi_l\sin\theta_l \\ -\cos\theta_l\sin\phi_l & \cos\phi_l & \sin\theta_l\cos\phi_l \\ \sin\theta_l & 0 & \cos\theta_l \end{bmatrix} \begin{bmatrix} \sin\theta\cos\phi \\ \sin\theta\sin\phi \\ \cos\theta \end{bmatrix}$$

$$\Omega_l = \begin{bmatrix} \cos\theta_l\cos\phi_l\sin\theta\cos\phi + \sin\phi_l\sin\theta\sin\phi - \cos\phi_l\sin\theta_l\cos\theta \\ -\cos\theta_l\sin\phi_l\sin\theta\cos\phi + \cos\phi_l\sin\theta\sin\phi + \sin\theta_l\cos\phi_l\cos\theta \\ \sin\theta_l\sin\theta\cos\phi + \cos\theta_l\cos\theta \end{bmatrix} \tag{38}$$

The function getRandomDirection(normal,dim) takes the unit normal vector and dimension as function arguments, and does all of the calculations explained above. It considers the dimension requested and returns unit direction vector.

```
const Point
ViewFactorBase::getRandomDirection(const Point & n,const int dim)
const
{
  Real theta_normal = acos(n(2));
  Real phi_normal{0};
  if (theta_normal!=0)
    if (n(1)<0)
      phi_normal = 2 * _PI-acos(n(0)/sin(theta_normal));
    else
      phi_normal = acos(n(0)/sin(theta_normal));
  const Real theta_local = -theta_normal;
  const Real phi_local = -phi_normal;
  Real
Rlocal[3][3]={{(cos(theta_local)*cos(phi_local)),sin(phi_local),(-
cos(phi_local)*sin(theta_local))},{(-
cos(theta_local)*sin(phi_local)),cos(phi_local),(sin(theta_local)*
sin(phi_local))},{sin(theta_local),0,cos(theta_local)}};
  Real theta{0},phi{0};
  const Real rand_phi = std::rand() / (1. * RAND_MAX);
  const Real rand_theta = std::rand() / (1. * RAND_MAX);
  switch (dim)
    case 2:
      theta = _PI/2;
      phi = 2 * _PI * rand_phi;
      break;
    case 3:
      theta = 0.5 * acos(1 - 2 * rand_theta);
      phi = 2 * _PI * rand_phi;
      break;
  const Point
dir_global(sin(theta)*cos(phi),sin(theta)*sin(phi),cos(theta));
  const Point
dir_local((Rlocal[0][0]*dir_global(0)+Rlocal[0][1]*dir_global(1)+R
local[0][2]*dir_global(2)),

(Rlocal[1][0]*dir_global(0)+Rlocal[1][1]*dir_global(1)+Rlocal[1][2
]*dir_global(2)),

(Rlocal[2][0]*dir_global(0)+Rlocal[2][1]*dir_global(1)+Rlocal[2][2
]*dir_global(2)));
  return dir_local;
}
```

3.4.9 TESTING POINT ON ELEMENT SIDE

Positions of intersection point and source point of MC rays are the most important information to calculate view factor between surfaces. Since random numbers are used in MC sampling, intersection point or source point might be in any coordinate. To decide whether a ray will be counted or not it is necessary to know their exact coordinates to understand if the point is inside or outside the element side. To test a point on element side, area can be used as the criterion. Unlike using center point to calculate the area of an element side, discussed previously in function getArea(), an arbitrary point lying on the same plane with element side is used in area calculations. If the point is inside, then the total area of triangles will give the area of element side. On the other hand, if it is outside then the total area will be greater than the actual area of element side. Therefore, the total area can be used as a criterion/parameter to check whether a point lies on the element side or not.

In Figure 3.17, for a 4-noded element side with a point, p, is shown. First, four vectors from the nodes to the point are created. Afterwards, areas of triangles, $A_1,\ A_2,$ $A_3,\ A_4$, are calculated by using two neighbor vectors, forming the sides of triangle, in equation (33). For the case shown in Figure 3.17, the total area is expected to be equal to the actual area of the element side, meaning the point is inside.

In Figure 3.18, for the same element side, a different point is defined. Areas are calculated in as previously discussed; however, in this case the total area is greater than the side area, which means the point is outside.

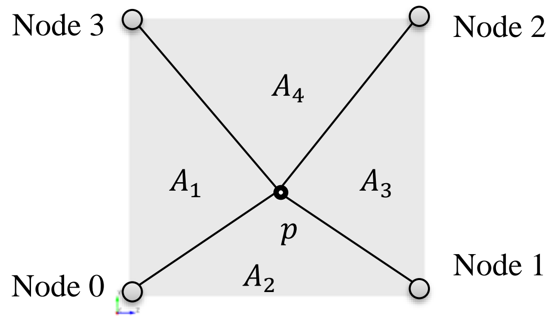

Figure 3.17 An arbitrary point on element side

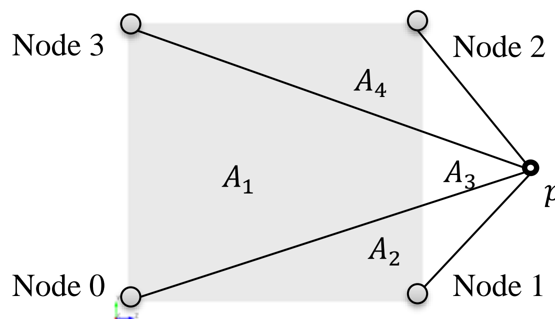

Figure 3.18 An arbitrary point out of element side

The function isOnSurface(point,sideMap) uses the discussed logic. It takes point and side_map as function arguments and tests if the point is on the element side. The function return type is boolean, e.g. if the point is on the side, it returns "true", otherwise returns "false". This function comes in useful for testing source and intersection points.

```
const bool
ViewFactorBase::isOnSurface(const Point &p, std::map<unsigned int,
std::vector<Point>> map) const
{
  const Point center{getCenterPoint(map)};
  Real elem_area = getArea(center,map);
  Real area = getArea(p,map);
  if ((area-elem_area)<_error_tol)
    return true;
  else
    return false;
}
```

3.4.10 SAMPLING RANDOM POINT ON ELEMENT SIDE

Besides sampling direction, multiple origins or source points are required to calculate view factors more accurately. Rays which are used in view factor calculations (see Figure 3.1), are emitted from 2D element sides, therefore random source points are sampled on the same side. One simple way to select a random origin point on a surface is drawing a circle around the geometric center of the side with radius that is large enough to expand to edges of the element side, shown in Figure 3.19, and then sampling a point inside the circle by randomly chosen radial position and angle.

The center point of element side and the radius of the circle can be easily calculated by equations (32) (30). The angular position of random point is similar to sampling direction in 3D. Since this random point lies on an element side, which is in *x-y* plane, the polar angle (θ) is assumed as constant angle of $\pi/2$. By making a small modification for azimuthal angle (ϕ), getRandomDirection() function can be used to find direction in 2D as well.

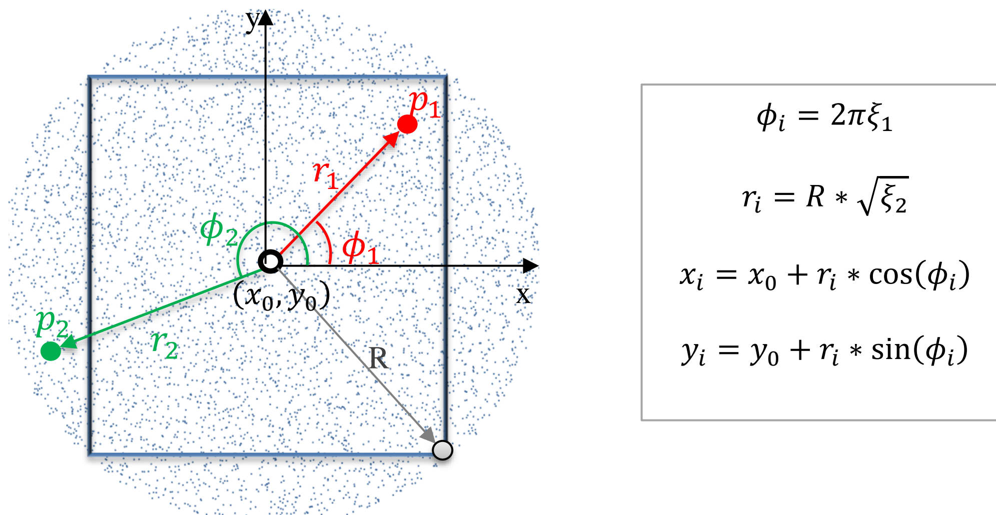

Figure 3.19 Uniform distribution on a circle surrounding the element side

The ϕ has uniform distribution, and it can be sampled over 2π by using pseudo-random numbers. The radial position of random point needs to be sampled over circle radius, R. To make radial position distribution uniform, sampling needs to be done according to inverse square law which states that a physical quantity or intensity is inversely proportional to the square of the distance from its source in space. This is similar to using cosine distribution for θ in 3D direction sampling to get a uniform distribution. Once the radial and angular position of point is found, they are converted to global cartesian coordinate system to be used in calculations.

As mentioned before, the random points are chosen to be in a circle that surrounds the element side. However, since the element side is not circular, it is possible that some points will be outside the element side. For example, in Figure 3.19, point p_2 is not on the element side and thus it is rejected as an origin point. This method is termed rejection method, in which first of all, points are chosen randomly, and then tested whether they are inside the domain of interest.

```
const Point
ViewFactorBase::getRandomPoint(std::map<unsigned int,
std::vector<Point>> map) const
{
  const Point n = getNormal(map);
  const Point center{getCenterPoint(map)};
  Real rad{0},d{0};  //radius, distance
  for (size_t i = 0; i < map.size(); i++)
    Point p = map[i][0];
    d = (p-center).norm();
    if (d>rad)
      rad=d;
  while (true)
    const Real rand_r = std::rand() / (1. * RAND_MAX);
    const Real r =rad * std::sqrt(rand_r);
    const Point dir(getRandomDirection(n,2));
    const Point p(center + r*dir);
    if (isOnSurface(p,map))
      return p;
}
```

The function getRandomPoint(sideMap) takes side_map as argument, creates a circle and samples a random point on it. After testing the point is on the element side by utilizing isOnSurface() function, it accepts the point as origin if it is on element side, and rejects one that is not.

3.4.11 TESTING ORIENTATION OF ELEMENT SIDES

Monte Carlo technique is one of the most computationally expensive numerical methods, and finding a way to speed up the calculations and decrease their memory usage is always favored. This can be done by avoiding unnecessary calculations and making reasonable assumptions. Therefore, to make view factor calculations more time and memory efficient, the orientation between surfaces are checked, and only relevant surfaces are selected.

The basic idea of surface picking is checking if two different surfaces facing each other, and they are eliminated if they cannot view each other. In case they face each other, MC simulations are initiated. This is done for all surface pairs in a geometry, using the surface normal as a main reference to check the orientation of surfaces.

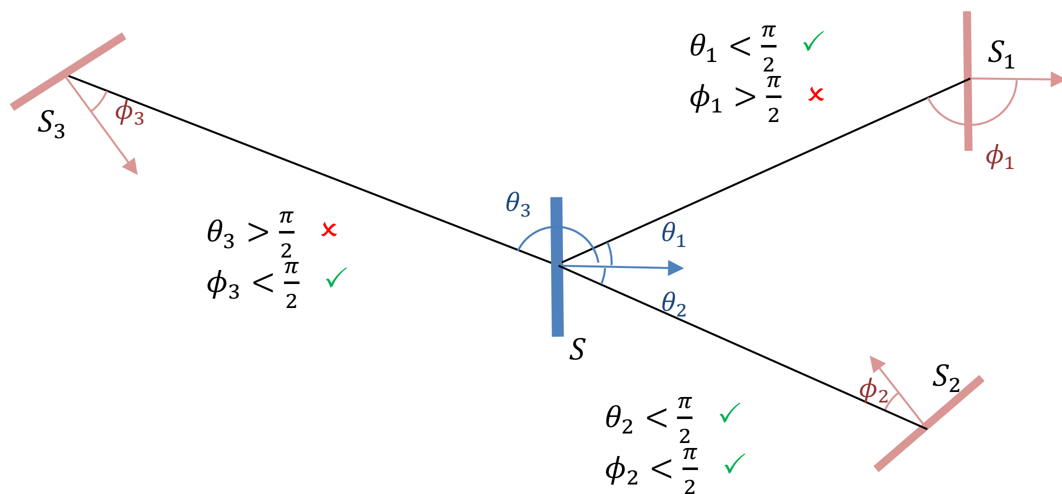

Figure 3.20 Surface orientation

Geometrically, surfaces are said to be turned towards each other if and only if the angles between surfaces' normal and the line connecting the centers of the surfaces are smaller than $\pi/2$. In Figure 3.20, only the surfaces S and S_2 are facing each other because both angles θ_2 and ϕ_2 are smaller than $\pi/2$. These angles can be called as orientation angles.

The function isSidetoSide(sideMap,sideMap) is written to check surface orientation by using the previously defined angle criteria. It takes side_map for each surface as function arguments, calculates orientation angles and tests if they uphold $\pi/2$ criteria.

```
const bool
ViewFactorBase::isSidetoSide(const std::map<unsigned int,
std::vector<Point>> & master_side_map,
                             const std::map<unsigned int,
std::vector<Point>> & slave_side_map) const
{
  std::map<unsigned int, std::vector<Point>> master_map =
master_side_map;
  std::map<unsigned int, std::vector<Point>> slave_map =
slave_side_map;
  const Point master_normal = getNormal(master_side_map);
  const Point slave_normal = getNormal(slave_side_map);
  for (size_t i = 0; i < master_side_map.size(); i++)
  {
    const Point master_node = master_map[i][0];
    for (size_t j = 0; j < slave_side_map.size(); j++)
    {
      const Point slave_node = slave_map[j][0];
      const Point master_slave = (slave_node - master_node);
      const Point slave_master = (master_node - slave_node);
      const Real theta_master_slave =
acos((master_normal*master_slave)/(master_normal.norm()*master_sla
ve.norm())); //Radian
      const Real theta_slave_master =
acos((slave_normal*slave_master)/(slave_normal.norm()*slave_master
.norm()));  //Radian
      if (theta_slave_master<_PI/2 && theta_master_slave<_PI/2)
        return true;
    }
  }
  return false;
}
```

3.4.12 TESTING INTERSECTION OF ELEMENT SIDES

As discussed previously, it is considered that the rays used in calculations are emitted from the random source points on the sides, traveling along a line until they intersect another element side. The intersection point is a point that satisfies both line equation which ray follows and plane equation on which target element side lie. Since the direction vector is known, the line equation can be found. Furthermore, element side is basically a small area on a 2D infinite plane whose equation can be found by normal vector and any point given in plane. Solving the line equation and plane equation together gives the coordinates of the point at which a ray intersects the 2D plane on which element side is located. However, it might happen that the intersection point is not located in the element side. Once the intersection point is found, it should be tested whether it lies on element surface or not, which is done by isOnSurface() function.

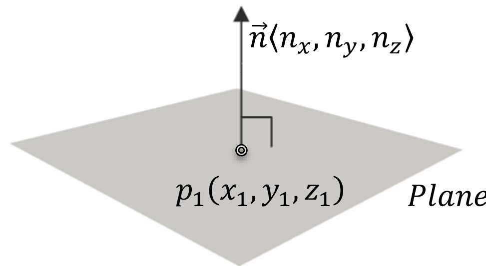

Figure 3.21 An arbitrary plane

In Figure 3.21, a plane with normal $\vec{n}\langle n_x, n_y, n_z\rangle$ and a point $p_1(x_1, y_1, z_1)$ are shown. The equation represents this plane is,

$$n_x(x - x_1) + n_y(y - y_1) + n_z(z - z_1) = 0$$

The unit direction vector $\vec{\Omega} = \langle \Omega_x, \Omega_y, \Omega_z\rangle$ shown in Figure 3.22 represents the ray's direction, and thus, using this vector and origin point, any point in ray's direction can be found.

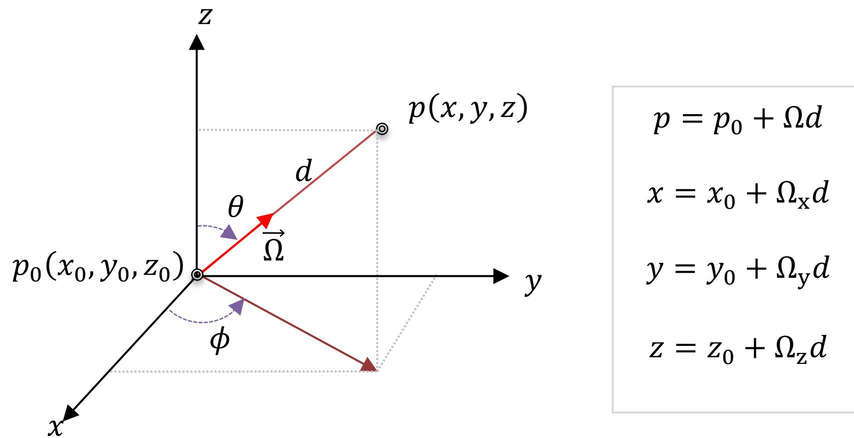

Figure 3.22 Intersection point in spherical coordinates

Figure 3.23 shows a random ray emitted from one plane to another. If there is a point that satisfies both the ray's and other plane's equation, then the ray will intersect the plane at that point, p. The only information known about point, p is the plane equation. If the distance, d, from the origin point was calculated, then the coordinates of intersection point can be found. d can be calculated by substituting coordinates of p into plane equation in terms of d and Ω.

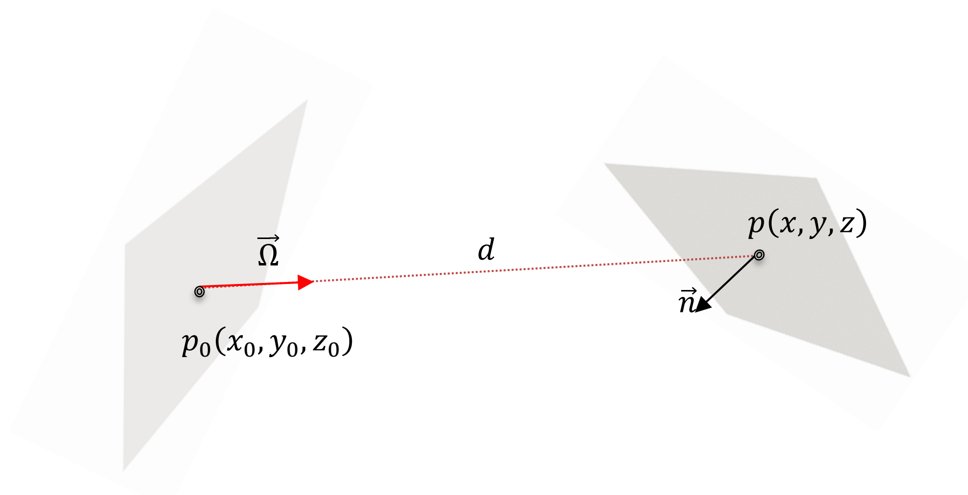

Figure 3.23 Representation of source and intersection point

Plane equation,

$$n_x(x - x_1) + n_y(y - y_1) + n_z(z - z_1) = 0$$

Line equations,

$$x = x_0 + \Omega_x d \qquad y = y_0 + \Omega_y d \qquad z = z_0 + \Omega_z d$$

Substitute line equations into plane equations,

$$n_x(x_0 + \Omega_x d - x_1) + n_y\left(y_0 + \Omega_y d - y_1\right) + n_z(z_0 + \Omega_z d - z_1) = 0$$

Solve for d,

$$d = \frac{n_x(x_1 - x_0) + n_y(y_1 - y_0) + n_z(z_1 - z_0)}{n_x\Omega_x + n_y\Omega_y + n_z\Omega_z} \tag{39}$$

Then, the coordinates of intersection point are calculated, $p(x, y, z)$

$$x = x_0 + \Omega_x d$$
$$y = y_0 + \Omega_y d \tag{40}$$
$$z = z_0 + \Omega_z d$$

Finding the intersection point is not enough because the element side is just a region in the plane. For the intersection point to be used in view factor calculations, it must be on the element side. For example, a point like the one shown in Figure 3.24 is not considered. The function isOnSurface() is used to check if a point is on the element side.

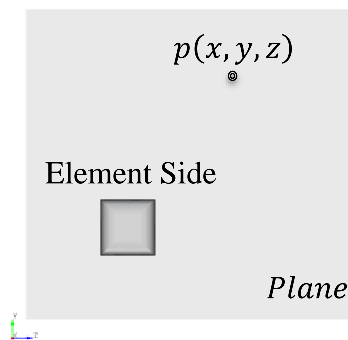

Figure 3.24 Testing intersection point on target surface

The function isIntersected(point,direction,sideMap) is used to test if rays are intersected with element sides. It takes the source point, ray's direction, and side map of element side wanted to be checked. The isIntersected() is a Boolean function, meaning If a ray intersect element side, it returns true. Otherwise, it returns false.

```
const bool
ViewFactorBase::isIntersected(const Point & p1,
                              const Point & dir,
                              std::map<unsigned int,
                              std::vector<Point>> map) const
{
  const Point n = getNormal(map);
  const Point pR = getRandomPoint(map);
  Real d = (n*(pR-p1))/(n*dir);
  const Point p2(p1 + d*dir);
  if (isOnSurface(p2,map))
    return true;
  else
    return false;
}
```

3.4.13 TESTING VISIBILITY OF ELEMENT SIDES

Because obstacles can influence the view factors, another important thing that needs to be checked is blocking surfaces. As mentioned before, the rays are considered active until they reach a surface. View factors are affected by intermediate surfaces between the source point and target surface because they will prevent radiating sides from viewing each other. The distance to target boundary d_{target}, shown in Figure 3.25, can be calculated since target boundary is predefined in input file.

Visibility testing requires all element sides in a geometry to be checked. The algorithm calculates the distances to all elements that might be struck by rays. If a shorter distance than the one to target is detected, it is understood that there is a blocking surface. Then the ray is removed from view factor calculations.

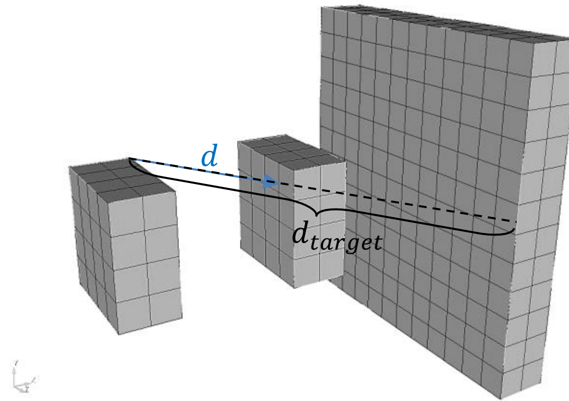

Figure 3.25 Testing visibility of target surface

The function, isVisible(sideMap,sideMap), is used to test if there is a blocking surface between the origin and target element side. It loops over all element sides in mesh and finds potential target elements that are within along path of ray. The distance from ray's origin to potential target element side is needed to understand whether it is blocking the actual target element by comparing it with d_{target}.

```
const bool
ViewFactorBase::isVisible(const std::map<unsigned int,
std::vector<Point>> & master_side_map,const std::map<unsigned int,
std::vector<Point>> & slave_side_map) const
{
  if (isSidetoSide(master_side_map, slave_side_map) == false)
    return false;
  const Point master_center = getCenterPoint(master_side_map);
  const Point slave_center = getCenterPoint(slave_side_map);
  Real d1 = (master_center - slave_center).norm();
  Point dir = (slave_center - master_center)/d1;
  Real d2{0};

  for (const auto & t : _mesh.buildSideList())
  {
    auto elem_id = std::get<0>(t);
    auto side_id = std::get<1>(t);
    auto bnd_id = std::get<2>(t);
    Elem * el = _mesh.elemPtr(elem_id);
    std::unique_ptr<const Elem> el_side = el-
>build_side_ptr(side_id);
    std::map<unsigned int, std::vector<Point>> side_map;
    unsigned int n_n = el_side->n_nodes();
```

```
    for (unsigned int i = 0; i < n_n; i++)
    {
      const Node * node = el_side->node_ptr(i);
      Point node_p((*node)(0), (*node)(1), (*node)(2));
      side_map[i].push_back(node_p);
    }
    const Point side_center = getCenterPoint(side_map);
    d2 = (master_center - side_center).norm();
    if (isSidetoSide(master_side_map, side_map) &&
isIntersected(master_center, dir, side_map) &&
        d2 < d1)
    {
      return false;
    }
  }
  return true;
}
```

3.4.14 MONTE CARLO CALCULATIONS

The functions described so far perform calculations related to geometry, while providing the basis for MC simulation. View factor calculations done using Monte Carlo simulation relies on tracking rays and counting how many of them strike the desired element sides.

The number of rays and number of source points are input parameters for Monte Carlo simulations. UserObject model gives the user a chance to define both in the input file. In model, a separate member function, which is doMonteCarlo(), is defined in ViewFactorBase class for Monte Carlo calculations. The function takes number of rays, number of source points and side maps of source and target element sides as function argument. It calculates surface normal for both sides by getNormal(), samples random source point location by getRandomPoint(), samples random direction by getRandomDirection(). At the end, it calculates view factor as a ratio of total intersected rays to total number of rays and returns it. Figure 3.26 is flow chart for doMonteCarlo() function, and the one in Figure 3.27 is the flow chart for ViewFactor model.

```
const Real
ViewFactorBase::doMonteCarlo(std::map<unsigned int,
std::vector<Point>> master_side_map,
                             std::map<unsigned int,
std::vector<Point>> slave_side_map,
                             unsigned int _sourceNumber,
                             unsigned int _samplingNumber)
{
  const Point master_elem_normal = getNormal(master_side_map);
  unsigned int counter{0};
  Real viewfactor_per_elem{0};
  Real viewfactor_per_src{0};
  for (size_t src = 0; src < _sourceNumber; src++)
  {
    viewfactor_per_src = 0;
    const Point source_point = getRandomPoint(master_side_map);
    counter = 0;
    for (size_t ray = 0; ray < _samplingNumber; ray++)
    {
      const Point direction =
getRandomDirection(master_elem_normal);
      const Real theta =
acos((direction*master_elem_normal)/(direction.norm()*master_elem_
normal.norm())); // Radian
      if (theta < _PI/2)
      {
        if (isIntersected(source_point, direction,
slave_side_map)) // check Intersecting
        {
          counter++;
        }
      }
    }
    viewfactor_per_src = (counter * 1.0) / _samplingNumber;
    viewfactor_per_elem += viewfactor_per_src;
  }
  viewfactor_per_elem *= (1.0/_sourceNumber);
  return viewfactor_per_elem;
}
```

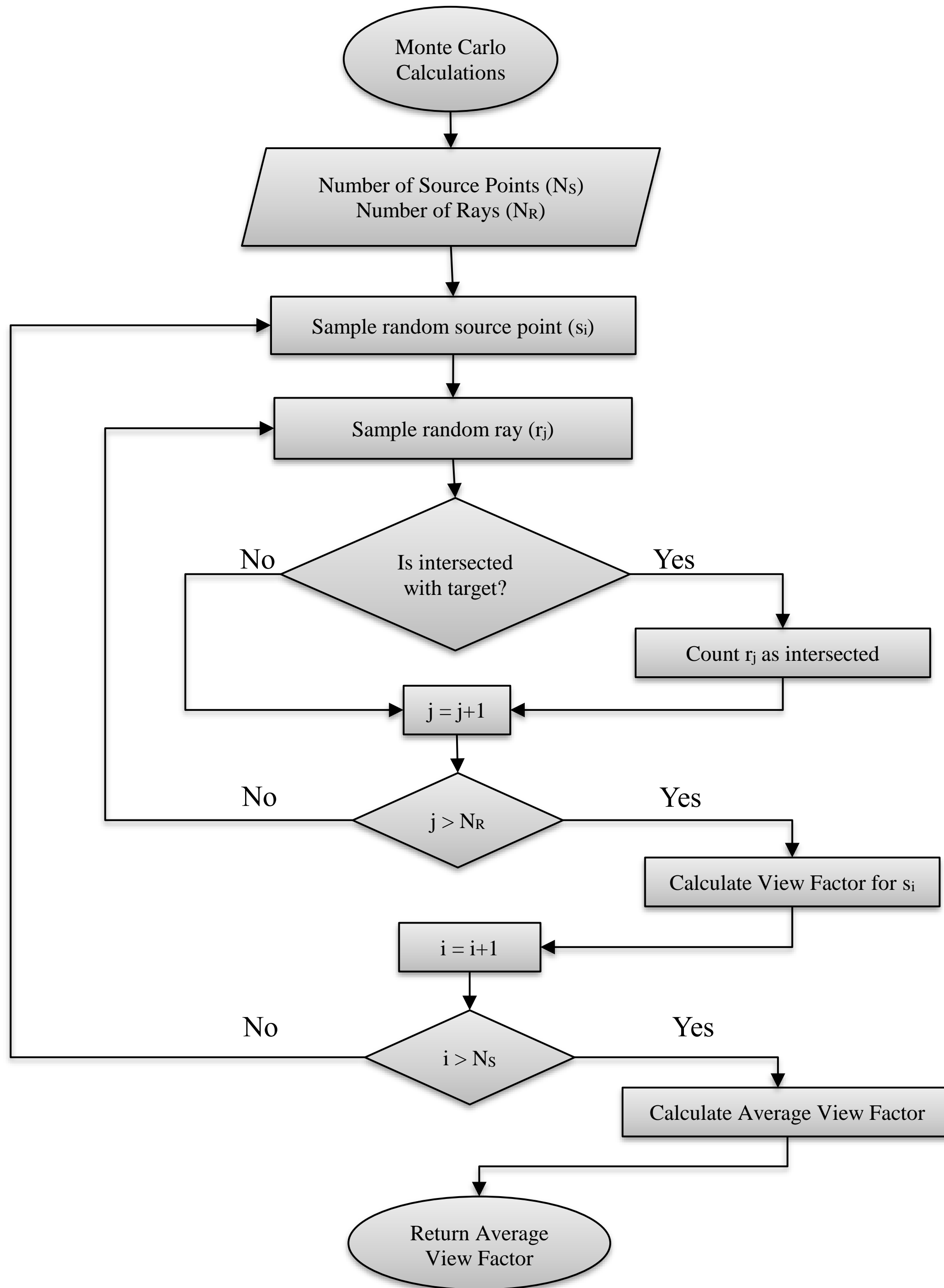

Figure 3.26 Flow chart for Monte Carlo calculations

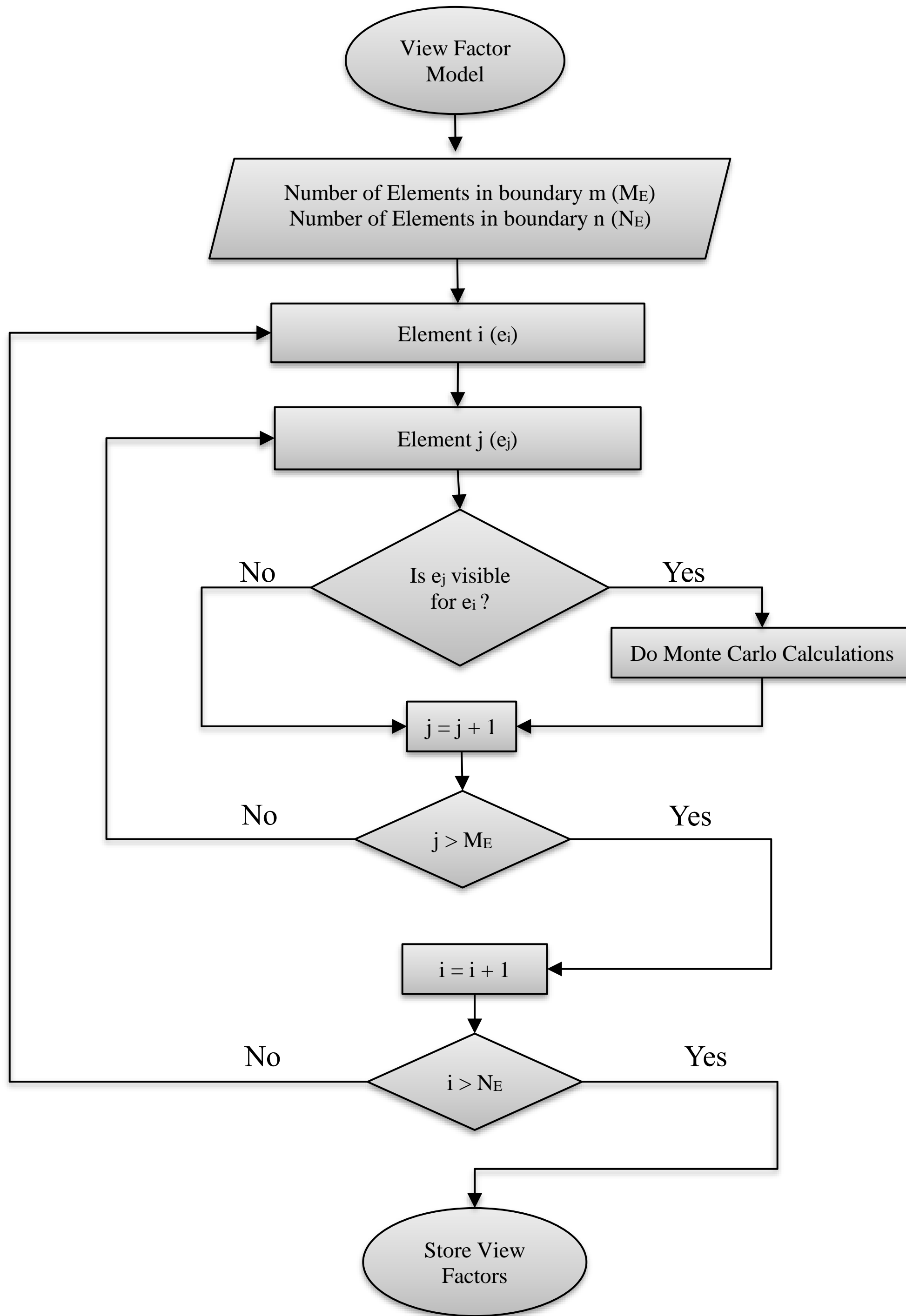

Figure 3.27 Flow chart for ViewFactor model

3.5 RADIATIVE HEAT TRANSFER MODEL

View factor calculations is only the first part of implementing this new radiative heat transfer model. When view factors between surfaces are known, then equation (9) can be solved. In MOOSE Mesh structure, block sides represent boundaries, and boundary conditions should be assigned to them. For radiative heat transfer calculations, a new boundary condition model "RadiativeHeatFluxBC" is added to MOOSE. It takes view factors from "ViewFactor" user object, calculates black body radiative heat flux and applies it as boundary condition for heat transfer calculations.

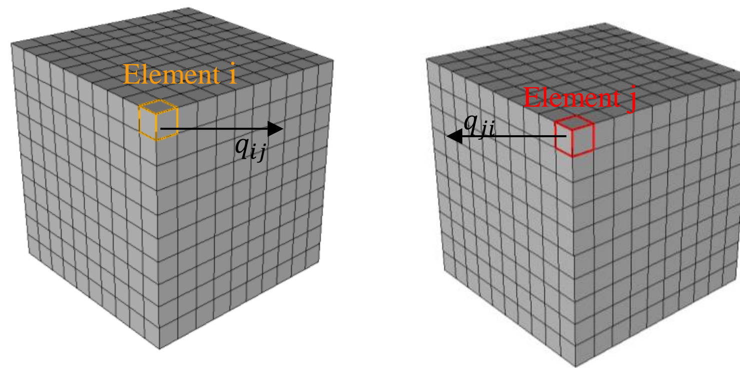

Figure 3.28 Radiative heat exchange between elements

Figure 3.28 shows outgoing fluxes from elements i and j. The net flux is calculated by subtracting all incoming fluxes from the outgoing fluxes, which is the basis of the new boundary condition model "RadiativeHeatFluxBC". The model loops over all elements in specified boundaries and calculates net heat flux for each element by pairing with all other elements, which is performed using following equation. The flow chart for radiative heat transfer model is shown in Figure 3.29.

$$q_{i,net} = q_{ij} - \sum_{j}^{n} F_{ij} q_{ji} = \sum_{j}^{n} F_{ij}\left(q_{ij} - q_{ji}\right) \tag{41}$$

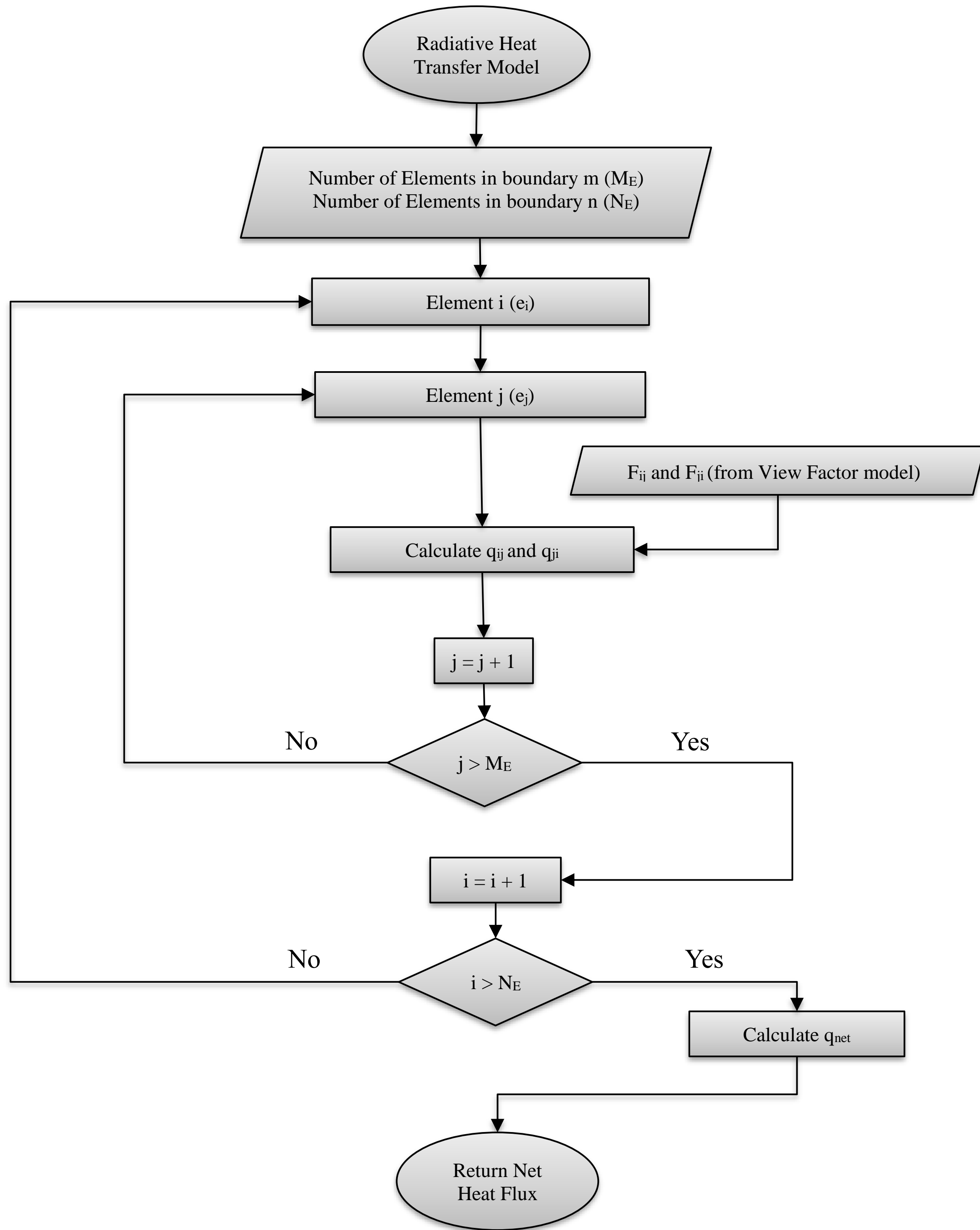

Figure 3.29 Flow chart for RadiativeHeatFluxBC model

CHAPTER 4

RESULTS AND DISCUSSION

The implemented view factor model is tested by using simple geometries. The finite element meshes are generated by using Trelis software. Different geometric parameters such as height, width, radius and the distance between surfaces, are used to generate geometries. Analytical view factor values ($F_{analytical}$) are calculated by using the formulas presented in Appendix D in textbook written by Modest [1]. The percentage error is calculated by following equation,

$$\%Error = 100 * \frac{|F_{analytical} - F_{calculated}|}{F_{analaytical}} \tag{42}$$

Since the view factors are calculated between the finite element surfaces, which are flat, not curved, the results obtained for flat geometries such as rectangles, disks, provide more insight about accuracy of ViewFactor model.

The radiative heat transfer model is tested by a case study which is pellet heating experiment. The current GapHeatTransfer model in MOOSE is used for comparison of results.

4.1 PARALLEL RECTANGLES

The rectangle surfaces illustrated in Figure 4.1 have h×w dimensions (h-height and w-width), separated from each other by distance, d, using hexahedral (HEX8) elements in the mesh. The results of calculations are presented by following table and figures.

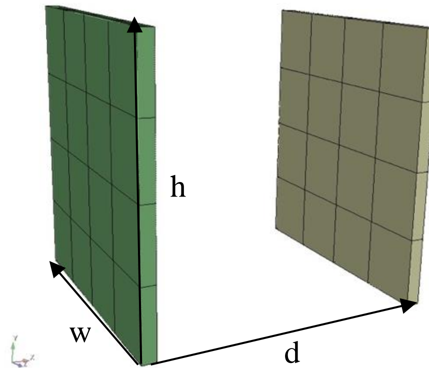

Figure 4.1 Geometry of parallel rectangles

Table 4.1 View Factors for h=2, w=2, d=2

	View Factors ($F_{calculated}$) for different number of sampling (N)					
Run	**10^2**	**10^3**	**10^4**	**10^5**	**10^6**	**10^7**
1	0.197500	0.198000	0.201075	0.199333	0.199678	0.199804
2	0.217500	0.187750	0.199625	0.200857	0.199034	0.199732
3	0.187500	0.201000	0.198500	0.198215	0.199734	0.199555
4	0.237500	0.190750	0.203650	0.198610	0.199910	0.199659
5	0.180000	0.199000	0.201100	0.199988	0.199708	0.199707
6	0.220000	0.196500	0.197725	0.198130	0.199606	0.199692
7	0.190000	0.207500	0.203075	0.200073	0.199661	0.199714
8	0.172500	0.203000	0.198375	0.199153	0.199683	0.199688
9	0.195000	0.199750	0.202125	0.199705	0.199738	0.199716
10	0.212500	0.198250	0.201750	0.200163	0.199603	0.199809
11	0.222500	0.198000	0.199550	0.201615	0.199968	0.199779
12	0.215000	0.198500	0.198900	0.200490	0.200102	0.199753
Mean F	0.203958	0.198167	0.200454	0.199694	0.199702	0.199717
Std Dev	0.019669	0.005118	0.001951	0.001060	0.000260	0.000069
Std Error	0.005678	0.001478	0.000563	0.000306	0.000075	0.000020
$F_{analytical}$	0.199825	0.199825	0.199825	0.199825	0.199825	0.199825
%Error	2.068530	0.829841	0.314911	0.065338	0.061460	0.053828

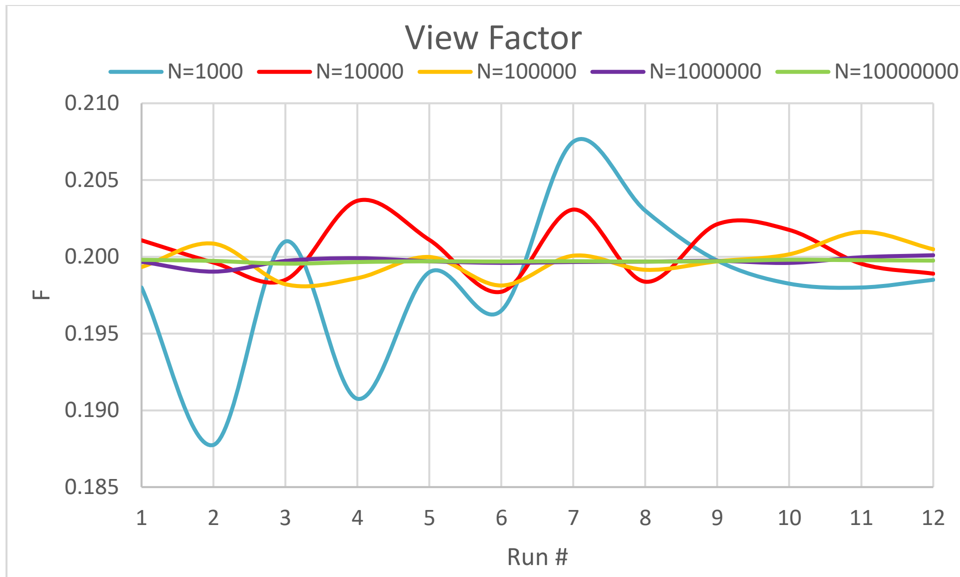

Figure 4.2 View factor for parallel plates for different sampling number

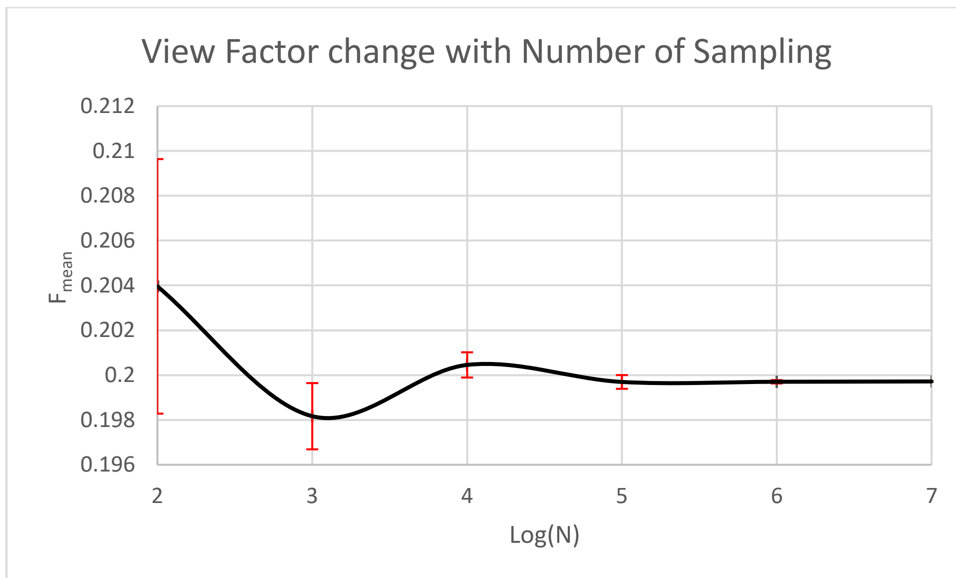

Figure 4.3 Change of average view factor with sampling number

Evidently, as the number of sampling increases, results become more precise (see Figure 4.3). Furthermore, the standard deviation of 12 runs, shown by the red bars in figure, and the absolute percent error decreases with increasing sampling as shown in Figure 4.4. At a sampling rate of 10^5, the standard deviation and standard error are

converged. Also, the absolute percent error drops below 0.1%, and thus, sampling number of $N=10^5$ can be used for similar geometries.

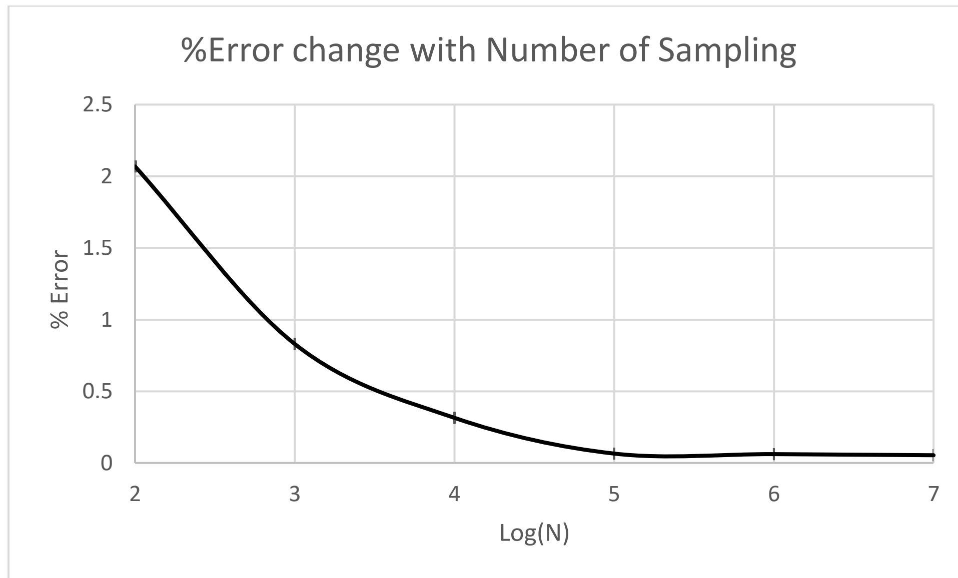

Figure 4.4 Change of percentage error with sampling number

The distance between rectangles is also an important parameter. In Table 4.2, calculated view factors are presented for square plates with different d/h ratios for $N=10^5$ rays. The error increases as d/h ratio is getting larger because as rays are spreading in radial direction, following Inverse Square Law (See section 3.4.10). Their probability of hitting the target surface decreases due to increased distance, coming from the geometric dilution due to point-source radiation into three-dimensional space. The rays used in the MC simulations in this study follow the inverse square law, since they are basically quantities emitted from a source point. It can be clearly seen from Figure 4.5 that the average view factor profile follows the inverse square law.

Table 4.2 View Factors for different plate dimensions

	d/h					
Run	**0.5**	**1.0**	**2.0**	**4.0**	**8.0**	**16.0**
1	0.416150	0.201075	0.067850	0.019475	0.005200	0.001525
2	0.409650	0.199625	0.068925	0.018975	0.004325	0.001175
3	0.413450	0.198500	0.069450	0.019500	0.005425	0.001425
4	0.414050	0.203650	0.068350	0.019900	0.004975	0.001475
5	0.414850	0.201100	0.069100	0.019300	0.005150	0.001550
6	0.417500	0.197725	0.068300	0.019150	0.005275	0.001275
7	0.412200	0.203075	0.066475	0.018975	0.005050	0.001375
8	0.414850	0.198375	0.070075	0.019300	0.005000	0.001300
9	0.409450	0.202125	0.067725	0.019075	0.005300	0.001150
10	0.412200	0.201750	0.068175	0.019425	0.004425	0.001225
11	0.414850	0.199550	0.068600	0.019375	0.005125	0.001475
12	0.411575	0.198900	0.068075	0.018750	0.005025	0.001125
Mean F	0.413398	0.200454	0.068425	0.019267	0.005023	0.001340
Std Dev	0.002468	0.001951	0.000921	0.000305	0.000331	0.000151
Std Error	0.000712	0.000563	0.000266	0.000088	0.000096	0.000044
$F_{analytical}$	0.415253	0.199825	0.068590	0.019107	0.004922	0.001240
%Error	0.446804	0.314911	0.239962	0.835866	2.040751	8.016045

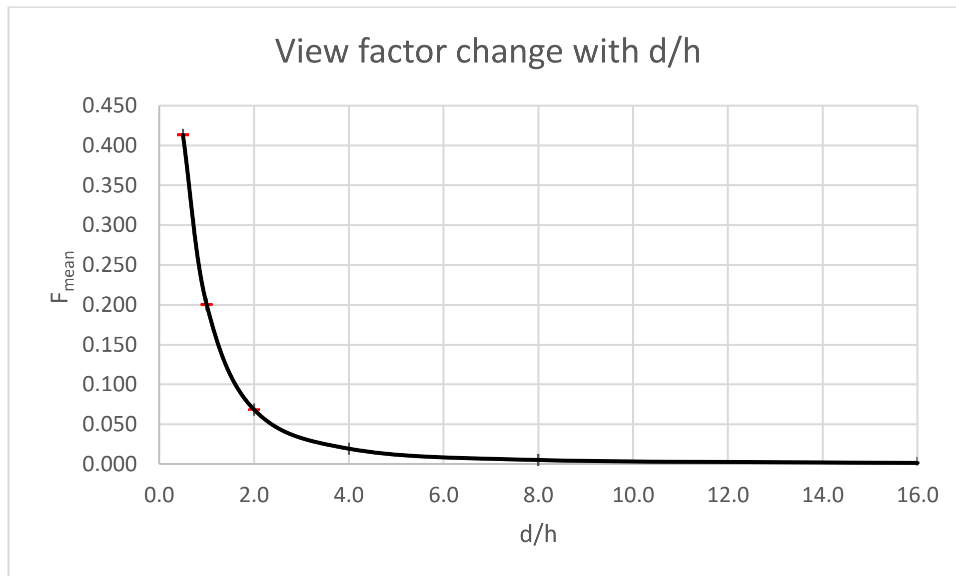

Figure 4.5 Change of average view factor with rectangle dimensions

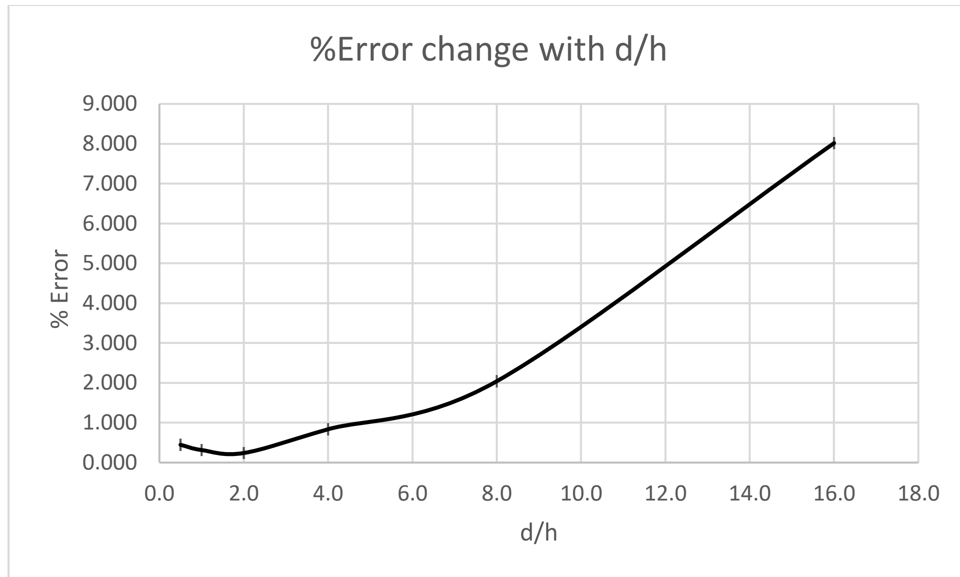

Figure 4.6 Change of percentage error with rectangle dimensions

4.2 PERPENDICULAR RECTANGLES

In the case of perpendicular rectangles, one has a height h, while the other has width w, both sharing a common edge with size d (see Figure 4.7), i.e., the rectangles have h×d and w×d dimensions.

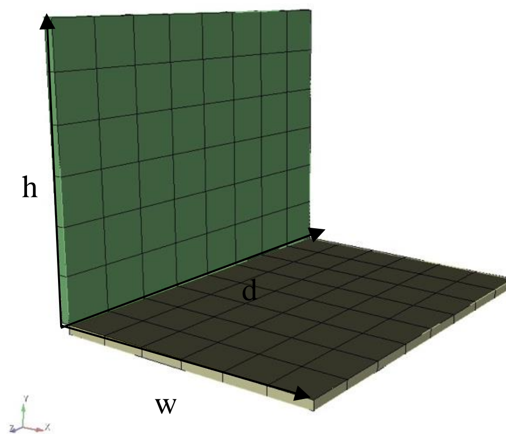

Figure 4.7 Geometry of perpendicular rectangles

Table 4.3 View Factors for h=3, w=3, d=4

	View Factors (F) for different number of sampling (N)				
Run	**10^2**	**10^3**	**10^4**	**10^5**	**10^6**
1	0.220000	0.221417	0.221892	0.222799	0.222488
2	0.253333	0.223083	0.219300	0.223012	0.219740
3	0.254167	0.228417	0.227242	0.220751	0.224597
4	0.246667	0.227583	0.215125	0.222885	0.225348
5	0.224167	0.234167	0.222967	0.219128	0.222387
6	0.247500	0.233833	0.224033	0.221029	0.219920
7	0.269167	0.219417	0.220642	0.221340	0.223036
8	0.270000	0.227167	0.218150	0.219530	0.222333
9	0.230000	0.211250	0.222925	0.223183	0.220520
10	0.223333	0.226833	0.220450	0.222948	0.217597
11	0.266667	0.216167	0.225700	0.223361	0.225435
12	0.245000	0.213333	0.223050	0.223543	0.220199
Mean F	0.245833	0.223556	0.221790	0.221959	0.221967
Std Dev	0.018056	0.007473	0.003321	0.001545	0.002441
Std Error	0.005212	0.002157	0.000959	0.000446	0.000705
$F_{analytical}$	0.2187	0.2187	0.2187	0.2187	0.2187
%Error	12.406683	2.220203	1.412742	1.490207	1.493675

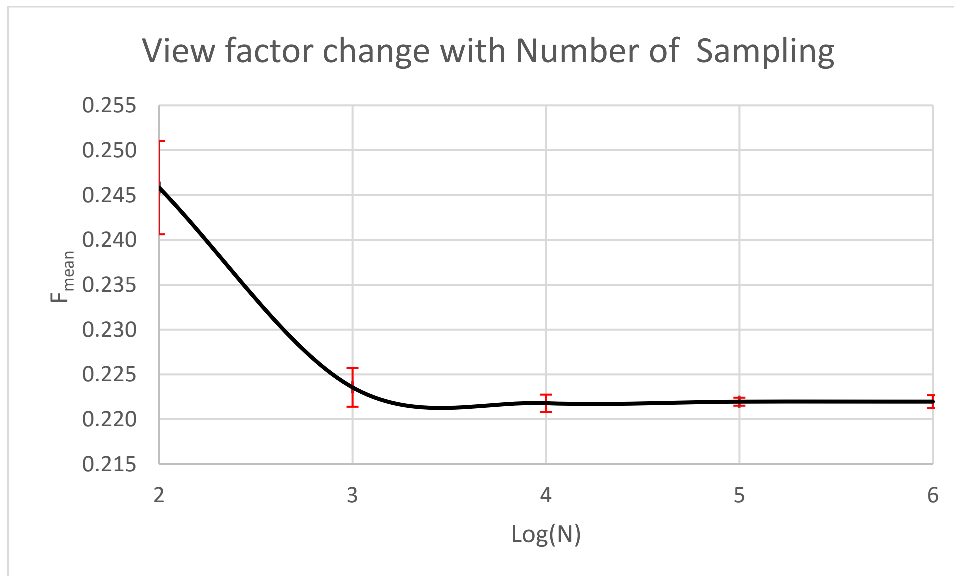

Figure 4.8 Change of average view factor with sampling number

Figure 4.8 shows the average view factor as a function of the number of rays, where the error bars represent their standard deviations. It is noticeable that the average view factor values fluctuate less compared to view factor values of the parallel rectangles. The percent error has the same profile. The reasonable sampling rate for this case is 10^4, because the view factor average values and their standard deviations, as well as the error are converged at this value.

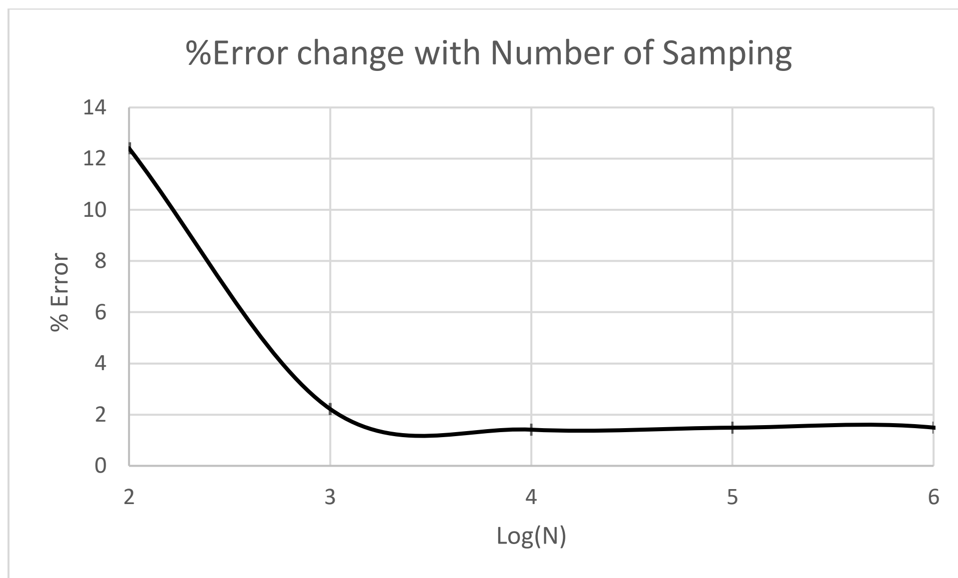

Figure 4.9 Change of percentage error with sampling number

The effect of the rectangles' dimensions on view factor, specifically the h/w ratio, is also investigated. The results are detailed in table and figure, showing that the average view factor increases as the dimension ratio gets larger. Note that the h/w is symmetric around 1, meaning increasing or decreasing the ratio by some amount will have the same effect on the calculations.

Table 4.4 View Factors for different rectangle dimensions

	h/w					
Run	**1.0**	**1.5**	**2.0**	**2.5**	**3.0**	**3.5**
1	0.221892	0.247080	0.259383	0.268727	0.275050	0.274044
2	0.219300	0.243660	0.260983	0.270260	0.267558	0.276206
3	0.227242	0.247080	0.258275	0.270291	0.269942	0.273187
4	0.215125	0.247080	0.262108	0.260344	0.271200	0.273187
5	0.222967	0.250358	0.262225	0.267273	0.275717	0.269248
6	0.224033	0.243667	0.259800	0.267922	0.266842	0.270155
7	0.220642	0.245670	0.262367	0.266995	0.272658	0.274875
8	0.218150	0.244012	0.258433	0.266995	0.270058	0.276685
9	0.222925	0.244012	0.254233	0.270313	0.272642	0.276999
10	0.220450	0.248107	0.259908	0.270260	0.268792	0.272384
11	0.225700	0.248107	0.254850	0.263211	0.271467	0.277737
12	0.223050	0.242250	0.261442	0.268322	0.265950	0.271606
Mean F	0.221790	0.245924	0.259501	0.267576	0.270656	0.273859
Std Dev	0.003321	0.002418	0.002708	0.003066	0.003082	0.002740
Std Error	0.000959	0.000698	0.000782	0.000885	0.000890	0.000791
$F_{analytical}$	0.2187	0.246	0.2592	0.2664	0.2707	0.2734
%Error	1.412742	0.031064	0.115966	0.441473	0.016131	0.168038

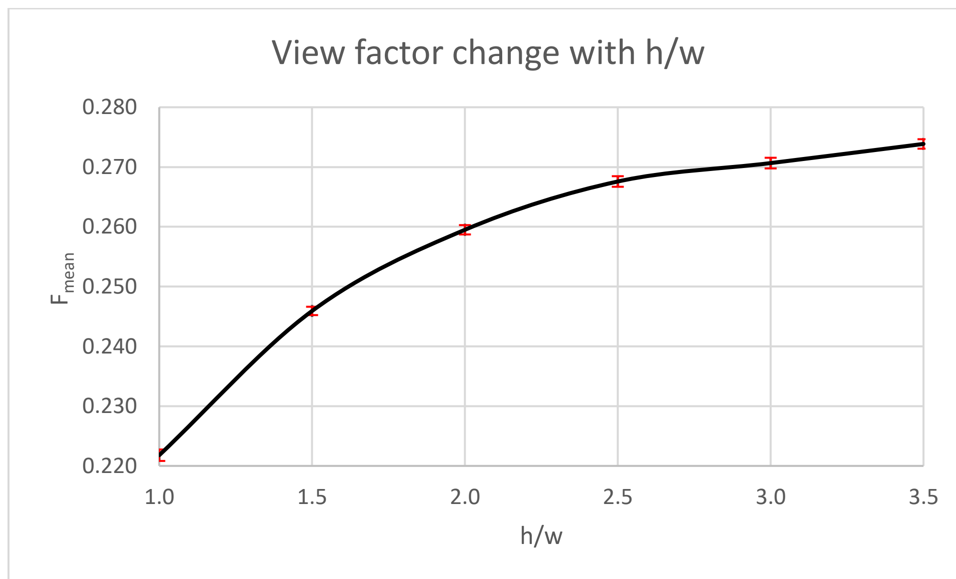

Figure 4.10 Change of average view factor with different rectangle dimensions

4.3 COAXIAL DISKS

Unlike the previous geometries, a circular geometry with tetrahedral (TET4) elements are used in view factor calculations.

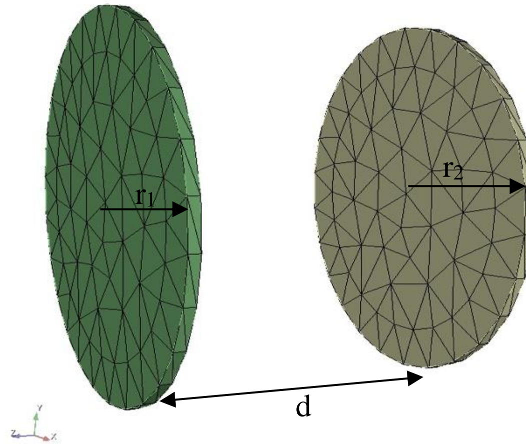

Figure 4.11 Geometry of coaxial disks

Coaxial disk geometries with radii r_1 and r_2, on a distance, d, are considered (see Figure 4.11), and the influence of the radii and distance on the view factor is investigated. $N=10^4$ rays are used in calculations.

Table 4.5 View factors for $r_1=2$, $r_2=2$, d=2

	Runs					
F_{12}	0.371386	0.371386	0.371386	0.371386	0.371386	0.371386
	0.370245	0.370245	0.370245	0.370245	0.370245	0.370245
Mean F			0.37128125			
Std Dev			0.00058474			
Std Error			0.00016880			
$F_{analytical}$			0.38196601			
%Error			2.79730681			

Table 4.6 View factors for different separation distance

	d/r					
	1.0	**2.0**	**3.0**	**4.0**	**5.0**	**6.0**
F_{12}	0.373800	0.164323	0.088396	0.053096	0.036141	0.024605
$F_{analytical}$	0.381966	0.171573	0.091673	0.055728	0.037088	0.026334
%Error	2.137890	4.225537	3.575299	4.723991	2.553609	6.567694

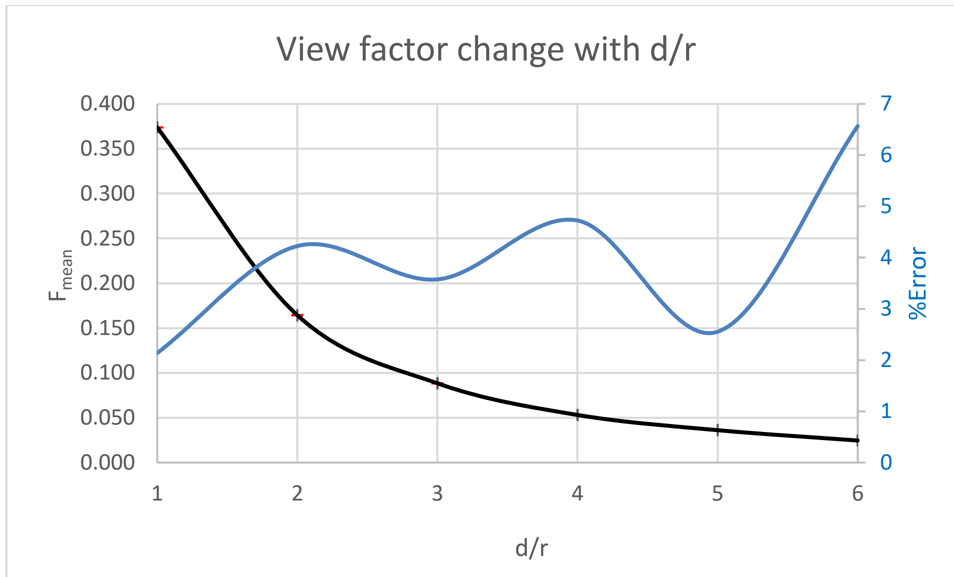

Figure 4.12 Change of average view factor with distance to radius ratio

Table 4.7 View factors for different disk dimensions

	r_1/r_2					
	1.0	**2.0**	**3.0**	**4.0**	**5.0**	**6.0**
F_{12}	0.167250	0.108821	0.070338	0.045622	0.030225	0.022339
$F_{analytical}$	0.171573	0.117218	0.075049	0.049485	0.034315	0.024936
%Error	2.519565	7.163402	6.278143	7.806354	11.91935	10.41428

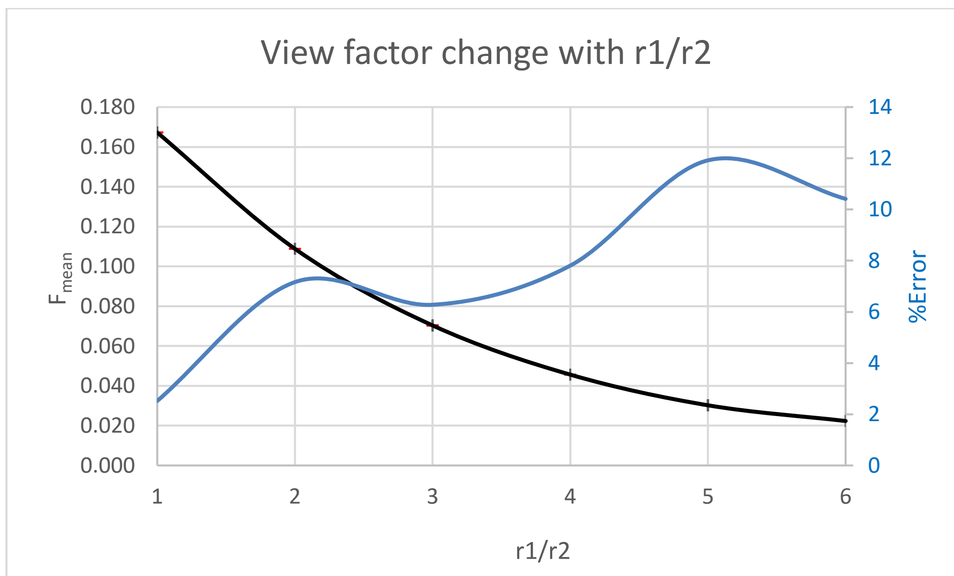

Figure 4.13 Change of average view factor with disk radius

4.4 COAXIAL CYLINDERS

Radiation surfaces are not necessarily always flat, they might have convex or/and concave areas. To study these animalities in the surfaces, coaxial cylinders, are considered in the calculations, shown in Figure 4.14. For these calculations $N=10^4$ rays are used.

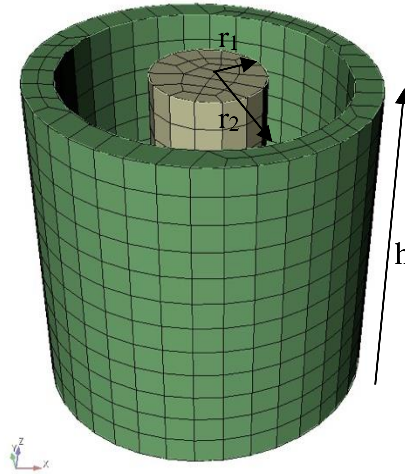

Figure 4.14 Geometry of coaxial cylinders

Table 4.8 View factors for $r_1=1$, $r_2=2.5$, $h=6$

	F_{12}			F_{21}		
Runs	0.829912	0.829912	0.829912	0.322021	0.323177	0.322091
	0.827846	0.827846	0.827846	0.323519	0.322761	0.323082
	0.829912	0.829912	0.829912	0.322639	0.322345	0.322516
	0.827846	0.827846	0.827846	0.321702	0.322905	0.323154
Mean F	0.8278304			0.3226572		
Std Dev	0.0012667			0.0005473		
Std Error	0.0003656			0.0001581		
$F_{analytical}$	0.8296384			0.3318552		
%Error	0.2179272			2.7719262		

4.5 CONCENTRIC SPHERES

The suggested model is also tested for concentric spheres, shown in Figure 4.15. Since inner sphere is within the outer sphere, it is expected that view factor between exterior of the inner sphere and interior of the outer sphere is equal to 1. Calculations were performed using $N=10^4$ rays, and the results are presented in Table 4.9.

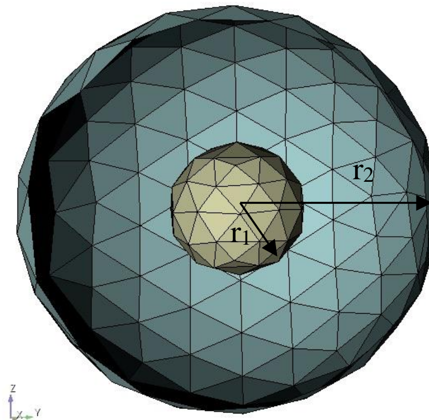

Figure 4.15 Geometry of concentric spheres

Table 4.9 View factors for $r_1=1$, $r_2=3$

	Runs					
F_{12}	1.00361	1.00466	1.00016	1.00353	1.00163	1.0063
	1.00175	1.00025	1.00451	1.00438	1.00264	1.00344
Mean F				1.003071667		
Std Dev				0.001854041		
Std Error				0.000535216		
$F_{analytical}$				1.0		
%Error				0.307166667		

4.6 CASE STUDY: MODELING OF PELLET HEATING EXPERIMENT

To test the performance of view factor model and radiative heat transfer model, ongoing pellet heating experiment at USC is modeled in MOOSE. The pellet is heated by joule heating via electrodes touching the pellet on opposite sides. Shown in Figure 4.16 is the half geometry of the experimental setup.

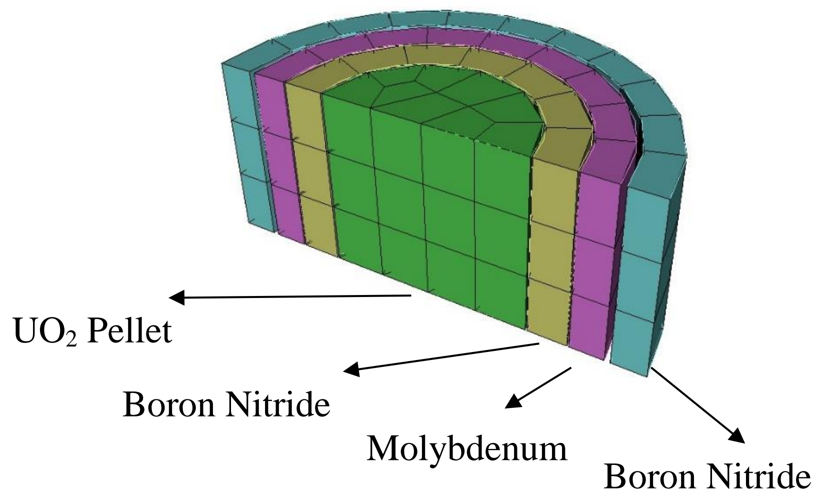

Figure 4.16 Geometry representation of experimental setup

There are three layers of materials around the pellet in purpose of insulation and stability. The dimensions and materials used in layers is given in Table 4.10.

Table 4.10 Geometrical parameters for experimental setup

	Material	Inner Radius(m)	Outer Radius (m)	Height (m)
Pellet	UO_2	-	0.005461	0.01
Tube 1	BN	0.005588	0.007747	0.01
Susceptor	Mo	0.007874	0.009652	0.01
Tube 2	BN	0.009906	0.011760	0.01

Temperature dependent thermal properties of UO_2 are used in calculations. A material model, using the equations given in Table 4.11, is implemented in MOOSE for UO_2. For other materials constant thermal properties given in Table 4.12 are used.

Table 4.11 Temperature Dependent UO_2 Thermal properties [13]

Thermal Conductivity (W/mK)	$\frac{100}{7.5408 + 1.7692 * 10^{-2}\,T + 3.6142 * 10^{-6}\,T^2 + 2.0239\frac{\exp(-16350/T)}{T^{2.5}}}$
Density (kg/m³)	$11049 - 0.334 * T + 3.9913 * 10^{-5}\,T^2 - 2.7649 * 10^{-8}\,T^3$
Specific Heat (J/kgK)	$193.218 - 2.6438 * 10^6\,T^{-1} + 0.325711\,T - 3.11971 * 10^{-4}\,T^2 + 1.1681 * 10^{-7}\,T^3 - 9.7523 * 10^{-12}\,T^4$

Table 4.12 Thermal properties of materials [14,15]

	Thermal Conductivity (W/mK)	Density (kg/m³)	Specific Heat (J/kgK)
BN	80	1900	810
Mo	138	10220	250

In the MOOSE model, the geometry is surrounded by a hemisphere surface to define ambient temperature (320 K) as boundary condition, see Figure 4.17.

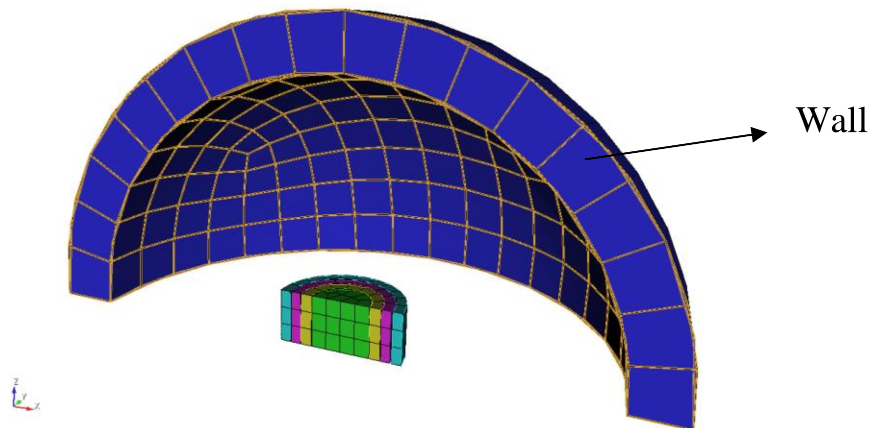

Figure 4.17 Computation model of experimental setup

Heat is generated in the pellet region by joule heating as a result of the voltage difference between electrodes.

Electrical Fourier Equation,

$$J_x = \sigma_x \frac{\Delta V}{\Delta x} \tag{43}$$

where J_x : current flux $[Amp/m^2]$

σ_x : electrical conductivity, $1/\rho_x$, $[1/\Omega m]$

ρ_x : electrical resistivity, $1/\sigma_x$, $[\Omega m]$

Δx : spatial coordinate in the direction of current flow $[m]$

ΔV : voltage difference $[volt]$

Joule Heating,

$$Q = J^2 \rho \tag{44}$$

where Q : joule heating power $[W/m^3]$

Then heat conduction equation with joule heating source term becomes,

$$\rho C_p \frac{\partial T}{\partial t} - \Delta \cdot k\Delta T - Q = 0 \tag{45}$$

Electrical conductivity of UO_2 is found from literature and assumed as constant. [16]

$$\sigma_x = 1\ \Omega m^{-1}$$

The applied voltage on electrodes is equal to 10V and constant during experiment. The volumetric heat generation is calculated as 82 MW/m^3 by equations (43) and (44) according to constant.

MOOSE currently has a gap heat transfer model, which is used to calculate heat transfer between fuel pellet surface and cladding inner surface. It is known that MOOSE's GapHeatTransfer can calculate heat transfer in small gaps accurately, so It can be used to verify RadiativeHeatFluxBC results.

For verification, the wall is removed from the geometry shown in Figure 4.17. Only concentric cylinders are used in simulations. A constant volumetric heat generation is defined in pellet. According to the results shown in Figure 4.18, the centerline temperature profiles are overlapping well. It can be concluded that RadiativeHeatFluxBC model is able to calculate accurately the radiative heat transfer between surfaces.

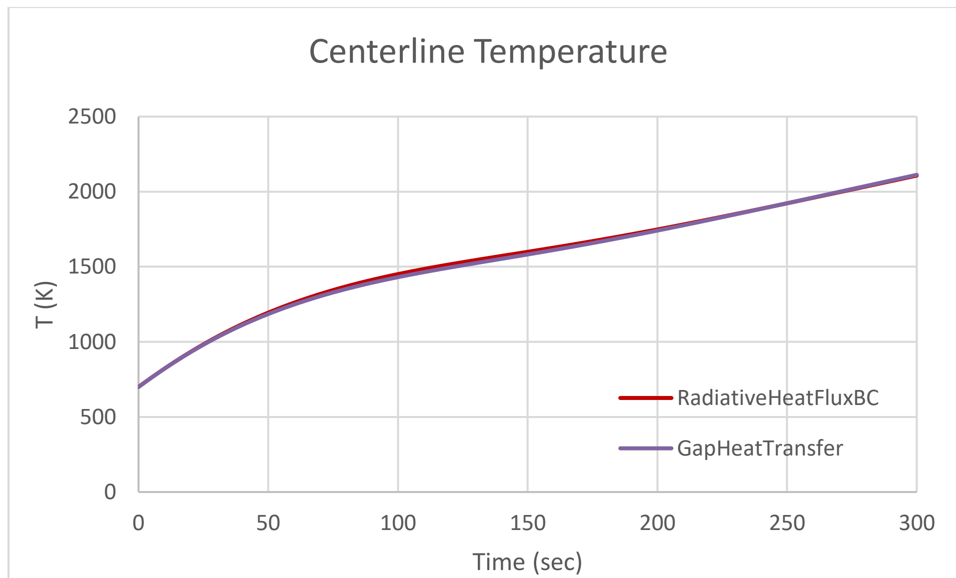

Figure 4.18 Pellet centerline temperature for only concentric cylinders

Next, calculations are repeated for the actual geometry shown in Figure 4.17. Constant voltage of 10V is used for this calculations. The centerline temperature change, radial and axial temperature profiles are shown in following figures.

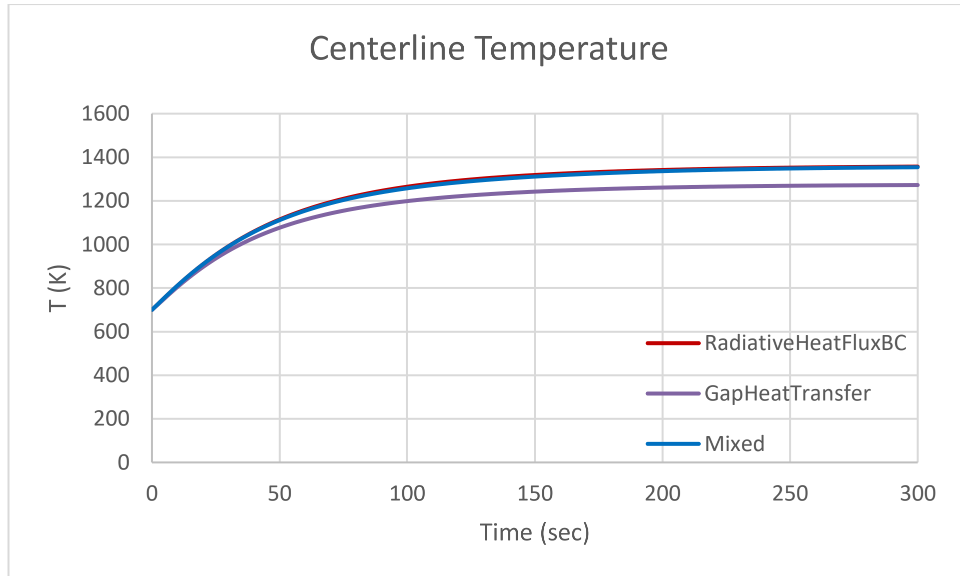

Figure 4.19 Pellet centerline temperature for computational geometry

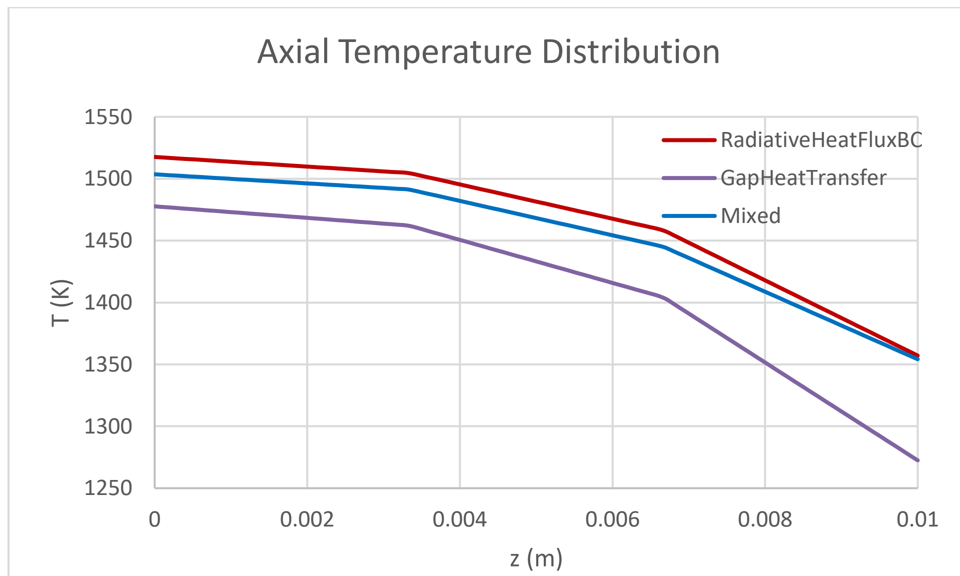

Figure 4.20 Axial temperature profile in pellet

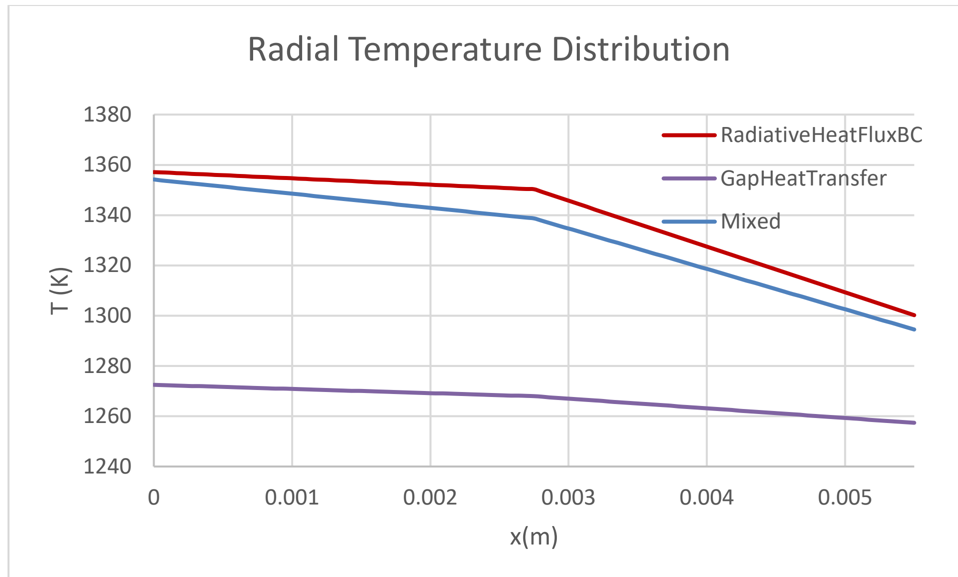

Figure 4.21 Radial temperature profile in pellet

All surfaces shown in Figure 4.17 are considered as radiating. The lines labeled by “Mixed” in figures represent the results obtained from using GapHeatTransfer model in concentric cylinders and RadiativeHeatFluxBC model for top surfaces in the same simulation. Mixed results overleap well with the RadiativeHeatFluxBC results.

GapHeatTransfer model makes assumptions for radiation heat transfer calculations. These are diffusion approximation and infinite parallel planes. These assumptions are reasonable for small gap geometries which view factor is almost unity. For larger gap geometries, view factor is smaller than 1, and thus GapHeatTransfer model might not provide accurate results. RadiativeHeatFluxBC model is more flexible and can provide more accurate results because it counts view factors.

In figures, RadiativeHeatFluxBC results are higher compared to GapHeatTransfer model results. The difference purely results from view factors. If the view factor is smaller than 1, less heat will be removed from surface. This causes an increase in temperature levels.

CHAPTER 5

CONCLUSION

Two new model have been implemented to MOOSE for view factor and radiative heat transfer calculations. In view factor model, the MC method is used and the user object "ViewFactor" is created. In radiative heat transfer model, calculations are done by assuming surfaces are black, and a boundary condition model "RadiativeHeatFluxBC" is added to MOOSE.

The MC method provides flexibility to calculate view factors for any kind of geometry. Although there are some drawbacks of MC method such as statistical error and computing time, by using high performance computers they could be minimized.

There is still work that can be done to improve implemented models. The view factor model is currently based on MC method. Other methods can be added as future work to give user option. The radiative heat flux model is calculating heat transfer by assuming surfaces are black. As a future work, it can be modified in order to use for radiative heat exchange between gray or diffuse surfaces, considering absorption, transmission and reflection.

BIBLIOGRAPHY

[1] Modest, M.F. 1993. *Radiative Heat Transfer*. McGraw-Hill. New York.

[2] Howell, J.R. 1998. *The Monte Carlo method in radiative heat transfer*. Journal of Heat Transfer 120 547-560.

[3] Metropolis, Nicholas, and Ulam, S. 1949. *The Monte Carlo Method*. Journal of American Statistical Association. 44-247 335-341.

[4] Junuthula Narasimha Reddy. *An introduction to the finite element method*, volume 2. McGraw-Hill New York, 1993.

[5] Derek Gaston, Chris Newman, Glen Hansen, and Damien Lebrun-Grandie. *Moose: A parallel computational framework for coupled systems of nonlinear equations.* Nuclear Engineering and Design, 239(10):1768–1778, 2009.

[6] JohnW. Peterson, Alexander D. Lindsay, Fande Kong, *Overview of the incompressible Navier-Stokes simulation capabilities in the MOOSE framework*, Advances in Engineering Software, 119:68-92, 2008.

[7] Santosh B. Bopche, Arunkumar Sridharan, *Determination of view factors by contour integral technique*, Annals of Nuclear Energy, 36: 1681-1688, 2009.

[8] Arvind Narayanaswamy, *An analytic expression for radiation view factor between two arbitrarily oriented planar polygons*, International Journal of Heat and Mass Transfer, 90: 841-847, 2015.

[9] Lei Yang, Wenzhen Chen, Lei Luo, Xinwen Zhao, *Calculation of radiation heat transfer view factors among fuel rod bundles based on CFD method*, Annals of Nuclear Energy, 71: 462-466, 2014.

[10] Matthew Barry, Justin Ying, Michael J. Durka, Corey E. Clifford, B.V.K. Reddy, Minking K. Chyu, *Numerical solution of radiation view factors within a thermoelectric device*, Energy, 102:427-435, 2016.

[11] M. Mirhosseini, A. Saboonchi, *View Factor calculation using Monte Carlo method for a 3D strip element to circular cylinder*, Energy Procedia 142 513-518, 2017.

[12] P.Mahanta, Subhash C. Mishra, *Collapsed dimension method applied to radiative transfer problems in complex enclosures with participating medium*, Numerical Heat Transfer, 42:4, 367-388, 2010.

[13] Uffelen P.V., Konings R.J.M., Vitanza C., Tulenko J. (2010) *Analysis of Reactor Fuel Rod Behavior*. In: Cacuci D.G. (eds) Handbook of Nuclear Engineering, 1519-1627.

[14] Technical Products Inc. *Boron Nitride Grade AX05 Material Specifications*, www.technicalproductsinc.com.

[15] International Molybdenum Association. *Molybdenum Properties, https://www.imoa.info/molybdenum/molybdenum-properties.php*

[16] Shoji Lida, *Electrical Properties of Non-Stoichiometric Uranium Dioxide,* Japanese Journal of Applied Physics, 4-11, 1